Evaluation and analysis of SMAP, AMSR2 and MEaSUREs freeze/thaw products in China

Jian Wang, Lingmei Jiang*, Huizhen Cui, Gongxue Wang, Jianwei Yang, Xiaojing Liu, Xu Su

State Key Laboratory of Remote Sensing Science, Jointly Sponsored by Beijing Normal University and Institute of Remote Sensing and Digital Earth of Chinese Academy of Sciences, Faculty of Geographical Science, Beijing Normal University, Beijing 100875, China

ABSTRACT

The surface seasonal freeze/thaw (F/T) signal detected by passive microwave remote sensing is very important for the water cycle, carbon cycle and climate change research. In this study, we evaluated and analyzed the Soil Moisture Active Passive (SMAP) L3 F/T product, Advanced Microwave Scanning Radiometer 2 (AMSR2) F/T product and Making Earth System Data Records for Use in Research Environments (MEaSUREs) F/T product over different regions in China, including the Genhe area in Northeast China, the Saihanba area in North China, and the Qinghai-Tibet Plateau (QTP) area. The overall accuracy of F/T products assessed with the 5 cm depth soil temperature is 90.38% for SMAP, 90.23% for AMSR2 and 84.73% for MEaSUREs in cold and humid temperate forest climates and the plateau continental climate area (Genhe, Tianjun, and Qumalai) where permafrost is distributed, and 76.64% for SMAP, 83.67% for AMSR2 and 77.37% for MEaSUREs in the cold plateau mountain climate and plateau continental climate area (Saihanba and Chengduo) with frozen ground distributed seasonally, respectively. The overall accuracy is 69.05% for SMAP, 76.5% for AMSR2 and 81.4% for MEaSUREs in the Ngari, Naqu, and Dachaidan regions belonging to arid and semi-arid climates. It can be seen that SMAP and AMSR2 achieve the best performance in the distributed permafrost area, the second-best performance in the seasonal distributed permafrost area, but the worst performance in the areas with arid and semi-arid climate types due to inconsistent F/T signals between water with small changes and temperature with apparent changes during the F/T transition. The MEaSUREs product showed almost the same performance in different regions, indicating that it was less affected by climate types and the distribution of frozen soil than SMAP and AMSR2 products. SMAP F/T product detected by L-band with long penetration and AMSR2 F/T product calibrated with 5 cm soil temperature could represent the 5 cm F/T, but the MEaSUREs F/T product was more likely to describe the surface F/T state due to calibrated with air temperature and the short penetration of 36.5 GHz. In mid-low latitude areas (Tianjun and Qumalai) with a short duration of snow cover days and a fast snowmelt, the effect of snow melting on F/T products was negligible. Moreover, the spring snowmelt affects the three F/T products in Chengduo, but the SMAP product is not affected by the winter snowmelt, whereas the AMSR2 product is affected by the winter snowmelt.

1. Introduction

As a part of the cryosphere, the spatial and temporal changes in the surface freeze/thaw (F/T) state have an important impact on hydrological, climatic and ecosystem processes (Kimball et al., 2004a; McDonald and Kimball, 2005). Approximately 50 million km^2 of land surface are subject to F/T changes every year, which mainly occur in the northern hemisphere at high latitudes and altitudes (Zhang et al., 2003b). The permafrost area in China is the third largest in the world, accounting for 22.3% of China's total land area (Zhou and Guo, 1982). In addition, permafrost in China is mainly distributed in Northeast

China, North China, Xinjiang and the Qinghai-Tibet Plateau (QTP). The beginning of the vegetation growing season is closely related to the thawing time of the surface, which controls the net primary productivity of vegetation and the carbon exchange between vegetation and the atmosphere (Kim et al., 2011b; Kim et al., 2012; Kimball et al., 2004b; Mcdonald et al., 2004). At the beginning of seasonal thawing, snow and glaciers begin to melt, which leads to an increase in river flow and possible flooding (Davitt et al., 2019; Jin et al., 2015; Kimball et al., 2001; Running et al., 1999). Surface F/T cycles that begin to appear in permafrost regions increase carbon and nitrogen emissions (Christensen, 2016; Gabrielle, 2007; Schuur and Abbott, 2011; Wang

---

* Corresponding author.
  E-mail address: jiang@bnu.edu.cn (L. Jiang).

et al., 2017a), which can lead to climate change uncertainties (Swindles et al., 2015). The F/T state affects soil physical properties and the soil hydrothermal cycle (Edwards et al., 2007). Monitoring the F/T state is very important for studying the hydrothermal distribution of the Earth system.

In the past few decades, a series of studies have been devoted to monitoring the surface F/T state by microwave remote sensing because microwave remote sensing is not affected by weather and atmospheric conditions, and it is very sensitive to dielectric constant changes in the surface. Many algorithms have been developed to monitor the surface F/T state using passive microwave remote sensing, including the double-index algorithm (Jin et al., 2015; Judge et al., 1997; Zhang and Armstrong, 2001; Zuerndorfer and England, 1992; Zuerndorfer et al., 1990), decision tree algorithm (Jin et al., 2009) and standard deviation algorithm (Han et al., 2015), and these algorithms are highly dependent on in situ data. The seasonal detection method (Derksen et al., 2017; Kim et al., 2011a; Rautiainen et al., 2018) and polarization ratio (PR)-based algorithm (Roy et al., 2015; Roy et al., 2017b) require more microwave remote sensing data that include both freeze and thaw states to determine the reference value of the F/T state. The modified seasonal threshold algorithm (MSTA) (Kim et al., 2017) requires one-year data to define the threshold of F/T. The discriminant function algorithms (Kou et al., 2018; Wang et al., 2018; Zhao et al., 2011) are established for various surface conditions with similar discriminant equations and different coefficients, but the fixed discriminant equation coefficients of each algorithm are not applicable to all regions.

Considering the importance of the F/T state in the water cycle, carbon cycle and climate change research, it is very important to evaluate the accuracy of F/T products. Therefore, F/T products based on passive microwave remote sensing estimation should be validated before further application. Some studies have evaluated different F/T estimation algorithms, such as comparing the three algorithms containing the double-index algorithm (Judge et al., 1997), decision tree algorithm (Jin et al., 2009) and discriminant function algorithm (Zhao et al., 2011) in China, where the discriminant function algorithm was found to have the highest accuracy at over 80% when compared to 0 cm land surface temperature (Chai et al., 2014). Since the successful launch of the Soil Moisture and Ocean Salinity (SMOS) mission and the NASA Soil Moisture Active Passive (SMAP) mission, an increasing number of studies have been devoted to the development of F/T monitoring algorithms in the L-band (Derksen et al., 2017; Rautiainen et al., 2018; Rautiainen et al., 2014; Rautiainen et al., 2016; Roy et al., 2015) due to its strong sensitivity to changes in soil permittivity. However, the validation data used in previous studies for the L-band F/T detected algorithm mainly come from the boreal forest and tundra in the northern hemisphere, such as Finland, Alaska, Quebec and other regions (Colliander et al., 2012; Davitt et al., 2019; Derksen et al., 2017; Lyu et al., 2018; Roy et al., 2015; Roy et al., 2017a; Roy et al., 2017b), including soil and air temperature data. Kim et al. (2019) assessed the performance of SMAP F/T products by using surface air temperature data from approximately 5000 global weather stations. However, the L-band is capable of determination of soil F/T states with deeper penetration, which requires further evaluation with soil temperature data. The F/T characteristics may be different since the distribution and characteristics of snow, soil and air temperature, and climate types between boreal and mid-low latitudes, where seasonal frozen soil is mainly distributed, are different. The L-band F/T detection algorithm, which has more sensitivity to the F/T transition, has been fully validated in the mid-high latitude regions. However, the capabilities of this algorithm in mid-low latitude regions require further validation. The discriminant function algorithm was further improved by parameterization with measurements from 46 in situ sites including China (CTP-SMTMN), USA (USA_NET, APEX), Canada (FLUXNET) and Finland (FMI) (Wang et al., 2018), and better than the dual-index algorithm and the decision tree algorithm over China (Chai et al., 2014). MSTA used V polarization brightness temperature (Tb) of 36.5 GHz

(Tb36.5 V) from AMSR2 satellite data to detect land surface F/T. Exploring the differences of F/T products based on AMSR2 Tb obtained by different algorithms is very important to understand land surface F/T retrieval. Therefore, the DFA, MSTA and the L-band F/T detection algorithms of SMAP are selected in this work and evaluated to analyze the applicability of different F/T detect algorithms over China.

In this study, the Advanced Microwave Scanning Radiometer 2 (AMSR2) F/T product, which is based on the DFA (Wang et al., 2018), the MEaSUREs F/T product (Kim et al., 2017) and the SMAP F/T product (Xu et al., 2018) are evaluated against the soil temperature at the 5-cm depth collected in China and the air temperature collected over QTP, respectively. The reason for using air temperature is to explore the consistency between F/T products and temperature of soil and air at low and middle latitudes based on limited data. Then, according to climate types and land surface parameters, we analyzed different F/T product behaviors in China. In Section 2, the study area with different observation networks and the SMAP, AMSR2 and MEaSUREs F/T algorithms and products are briefly described. In Section 3, an inter-comparison of F/T products with in situ data is presented. In Section 4, a discussion is given, which is followed by the conclusion section in Section 5.

2. Materials and methods

In this section, the study area, in situ data, SMAP F/T product, AMSR2 F/T product, and MEaSUREs F/T products used in this study are described.

2.1. Study area and ground data

The in situ soil temperature and soil moisture measurement monitoring network were collected from three regions located in Northeast China, North China and the QTP area, and each monitoring network contained a number of stations ranging from 1 to 16. The in situ air temperature data were collected from four monitoring networks, including Dachaidan, Tianjun, Qumalai, and Chengduo in the QTP area. The study areas in Northeast China and North China refer to the regions of Genhe and Saihanba, respectively. The study areas in the QTP include the regions of Ngari, Naqu, Dachaidan, Tianjun, Qumalai, and Chengduo. Except for the Ngari (Su et al., 2011) and Naqu (Qin et al., 2013; Yang et al., 2013) region data that were collected from the Third Pole Environment Database (http://en.tpedatabase.cn/), the ground measurement data of other regions used in this work were obtained by the Beijing Normal University observation network (Cui et al., 2017; Jiang et al., 2017). Fig. 1(a) shows the distribution of the study regions, geocryological regions and classifications in China (Qiu et al., 2000). The map of geocryological regions and classifications in Fig. 1(a) comes from the Environmental and Ecological Science Data Center of West China, National Natural Science Foundation of China (http://westdc.westgis.ac.cn). Fig. 1(b) shows the land cover map and distribution of stations in eight study areas. The 2010 land cover map is from Globe-Land30-2010, which is provided by the National Geomatics Center of China based on the integration of pixel- and object-based methods with knowledge and over 10,000 Landsat satellite images. The overall accuracy of this land cover map is over 80% (Chen et al., 2015) (http://www.webmap.cn/mapDataAction.do?method=globalLandCover).

Genhe area is a cold and humid temperate forest climate and a continental monsoon climate located in Northeast China and the northern part of the Great Khingan Range, where the northernmost and coldest areas in Inner Mongolia and land cover are mainly woodland, grassland and agricultural land. In this typical distribution area of permafrost in China, phaeozem is a valuable soil resource that is widely distributed over the Genhe area, and the F/T cycle will lead to soil erosion and other problems for the phaeozem. Simultaneously, the Genhe area contains the largest wetland in China, and the acquisition of high-precision land surface F/T products is of great significance to
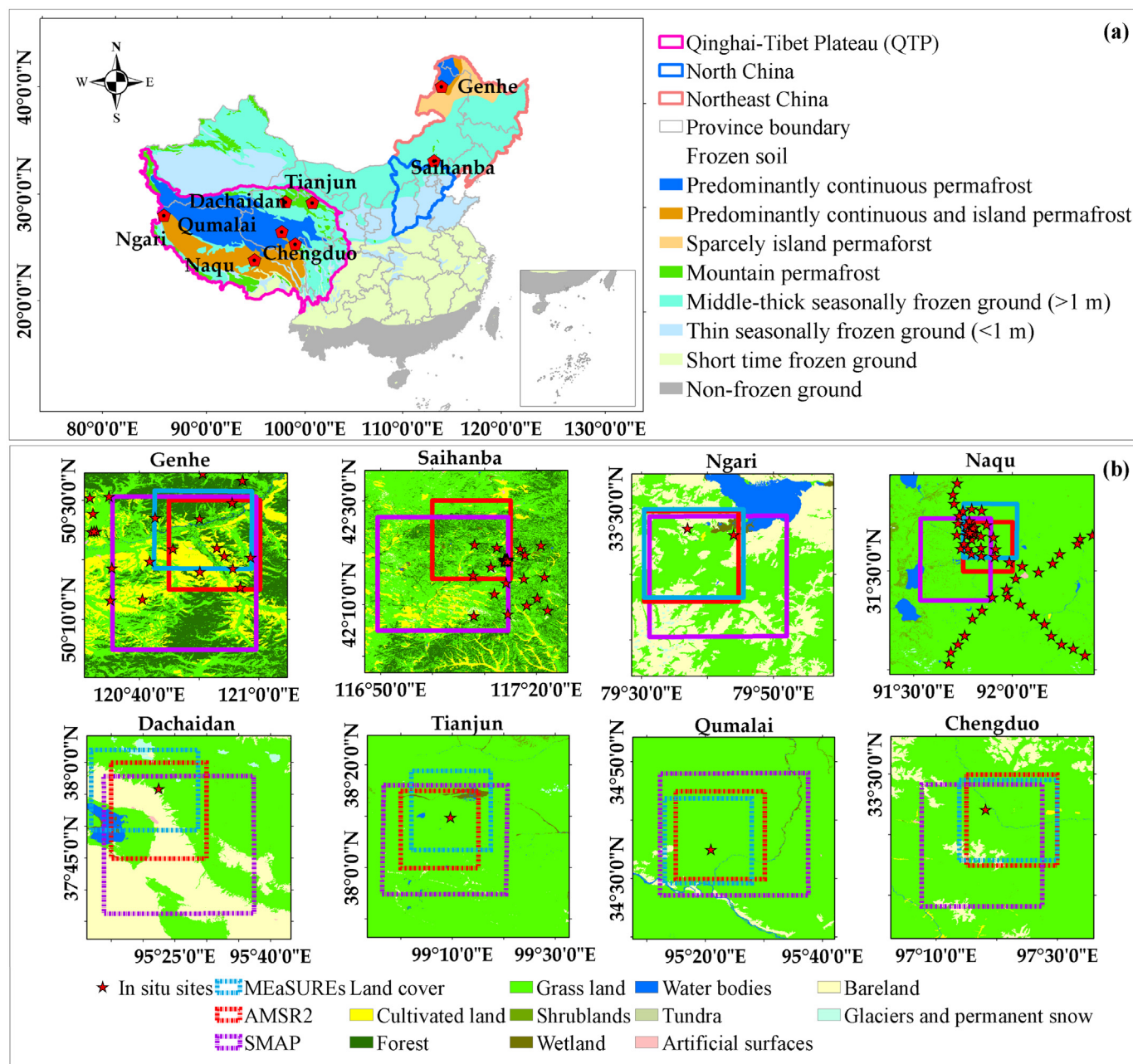
Fig. 1. Distribution of permafrost and study area with land cover map (http://www.webmap.cn/mapDataAction.do?method=globalLandCover) over China. (For interpretation of the references to color in this figure, the reader is referred to the web version of this article.)

studies of the release and accumulation of organic matter in wetland ecosystems. The in situ observation data of Genhe used in this study were obtained from the Beijing Normal University observation network (BNU-NET) (Cui et al., 2017). BNU-NET is deployed in the Genhe area (50°–51°N, 120.25°–121°E) and has been observed since July 16, 2013. Until August 2019, there were 22 sites in total whose soil moisture and soil temperature are measured by the Em50 ECH2O EC-5TM probes (Decagon Devices, Inc., Washington, USA) and XST probes (BJ XST Co., Ltd., www.xingshitu.com) every 30 min at depths of 3 cm, 5 cm, 10 cm and 20 cm below the surface.

Saihanba, located in the Xiaoluan Watershed basin in North China, has a semi-arid and semi-humid climate that is mainly covered by forest and grassland, and the elevation ranges from 1100 to 1800 m, with widely distributed seasonally frozen ground. The largest human-made forest in China is located here (Yang et al., 2019), with a very unique alpine river source wetland, which contributes to a complete aquatic

ecosystem composed of forest, grassland, meadow, swamp and water bodies. Soil moisture and soil temperature data were obtained from a remote sensing comprehensive experiment of the carbon cycle, water cycle and energy balance: Dataset of Soil Moisture and Temperature in the Xiaoluan Watershed (42°–42.5°N, 117°–117.5°E), which contains a total of 30 stations and has been available since September 2018. The data were collected by the Em50 ECH2O EC-5TM probes and XST probes every 30 min at two depths of 5 cm and 10 cm, and the in situ data were calibrated based on the impact of soil texture.

The QTP covers an area of $> 2.57 \times 10^6$ km^2 in western China with an average altitude of 4000 m and complex terrain comprising permafrost and seasonally frozen ground. In recent decades, a warming trend has occurred in most areas of the QTP (Li et al., 2018; Liu and Chen, 2000; Qin et al., 2009; Wang and Liang, 2013). In situ soil temperatures were collected from Ngari in the area west of the QTP with in situ data from the Tibetan Plateau Observatory of plateau-scale

Table 1

Information on the in situ regions. N is the number of stations at each site; the land cover map is from GlobeLand30-2010. We measured the soil texture data of Genhe and Saihanba from laboratory measurements using a pipette method, while the soil texture data of other areas were collected from Data Center for Resources and Environmental Sciences, Chinese Academy of Sciences (RESDC) (http://www.resdc.cn).

Areas	Regions	N	Start End	Climate	Land cover	Soil texture (clay, sand)	Frozen soil
Genhe	Northeast China	9	March 2016 February 2018	Cold and humid temperate forest; continental monsoon	Forest Grassland	39%–44%, 6%–9%	Predominantly continuous and island permafrost
Saihanba	North China	7	September 2018 February 2019	Cold plateau mountain climate	Forest Grassland	9%, 79%	Middle-thick seasonally frozen ground (> 1 m)
Ngari	Western QTP	3	September 2015 August 2016	Cold arid	Bare land, Grassland	11%, 80%	Predominantly continuous and island permafrost; Middle-thick seasonally frozen ground (> 1 m)
Naqu	Central QTP	16	September 2015 August 2016	Cold semi-arid	Grassland	20%, 66%	
Dachaidan	Northeast QTP	1	March 2016 August 2018	Inland plateau desert	Bare land, Grassland	11%, 56%	Middle-thick seasonally frozen ground (> 1 m)
Tianjun	Northeast QTP	1	March 2016 August 2018	Plateau continental	Grassland	19%, 29%	Mountain permafrost
Qumalai	Northeast QTP	1	March 2016 August 2018	Cold	Grassland, Bare land	13%, 42%	Predominantly continuous permafrost
Chengduo	East QTP	1	March 2016 August 2018	Plateau continental	Grassland, Bare land	18%, 53%	Middle-thick seasonally frozen ground (> 1 m)

soil moisture and soil temperature (Tibet-Obs) (Su et al., 2011), Naqu in the middle of the QTP with in situ measurements obtained from the multiscale Soil Moisture and Temperature Monitoring Network in the central Tibetan Plateau (CTP-SMTMN) (Yang et al., 2013), and Dachaidan, Tianjun, Qumalai and Chengdu in the northeastern area of the QTP with an automatic measurement dataset of snow depth on the Tibetan Plateau (Jiang et al., 2017). The last four study areas also contain air temperature measurements.

In Fig. 1, the red box represents the pixel position of AMSR2, the purple box represents the pixel position of SMAP, and the blue box represents the pixel position of MEaSUREs. The pixel position represented by the dashed box contained both soil temperature and air temperature observation data, and the pixel position represented by the solid box only contained soil temperature data. Soil moisture and temperature were measured at a depth of 5 cm underground. The observed height of air temperature is 2 m. Considering the local overpass time, spatial resolutions and locations of the SMAP, AMSR2 and MEaSUREs pixels, we selected the average 5 cm depth soil temperature data of the stations located in the SMAP, AMSR2 and MEaSUREs pixel to validate the F/T products. Table 1 summarizes the main features of the eight study areas.

2.2. Satellite data

2.2.1. SMAP L3 F/T products

Since its successful launch in January 2015, SMAP has provided L-band radiometer data and radar data with a revisiting period of approximately 2–3 days, including half-orbits about the ascent (6:00 PM) and descent (6:00 AM). The SMAP instrument contained both an L-band radiometer (1.41 GHz) and an L-band radar (1.26 and 1.29 GHz), but the L-band radar stopped working on 7 July 2015 due to an instrument anomaly. SMAP provides daily global and northern hemisphere surface F/T products with spatial resolutions of 36 km and 9 km, respectively. In this study, to analyze the F/T algorithm and product performance of SMAP, global F/T products (version 2) with a 36-km spatial resolution without downscaling processing were selected for validation and analysis, which can be downloaded from https://nsidc.org/data/SPL3FTP/versions/2.

The SMAP F/T baseline detection algorithm based on the seasonal threshold algorithm identifies the surface F/T state through temporal changes in the normalized polarization ratio (NPR) of Tb. However, the baseline detection algorithm is not applicable in areas where the freezing days are < 20 days; SMAP F/T was detected by an MSTA in these areas using the single channel V polarized (SCV) brightness

temperature. MSTA-SCV is similar to that of Kim et al. (2017), except that SMAP used the L-band, not Ka-band. The SMAP F/T product of eight study areas was obtained based on baseline detection algorithm with NPR, so this algorithm will be described in detail. The NPR is defined by vertical (TbV) and horizontal (TbH) polarization responses to the change in the dielectric constant resulting from water changes when F/T occurs. NPR is defined as follows (Derksen et al., 2017):

$$NPR = (TbV - TbH)/(TbV + TbH) * 100 \qquad (1)$$

According to the seasonal threshold algorithm, the seasonal scale factor corresponding to time t is defined as follows (Derksen et al., 2017):

$$\Delta t = (NPR(t) - NPR(fr))/(NPR(th) - NPR(fr)) \qquad (2)$$

where NPR (t) is NPR at time t, and NPR (fr) and NPR (th) are NPRs obtained under frozen and thawed land surfaces, respectively. Finally, the F/T state of the land surface is obtained according to the following formula (Derksen et al., 2017):

$$\Delta t > T, thaw \qquad (3)$$

$$\Delta t < T, freeze \qquad (4)$$

The value of parameter T is fixed at 0.5. All the SMAP F/T products corresponding to the study area are obtained based on this baseline algorithm. Additionally, SMAP provides daily morning and afternoon F/T products. SMAP F/T products also include NPR, NPR (fr) NPR (th).

2.2.2. AMSR2 F/T product

The AMSR2 F/T detection algorithm is based on information that can reflect surface temperature and emissivity to detect the F/T state. The AMSR2 L3 Tb data with the spatial resolution of 0.25° used in this study is provided by the Japan Aerospace Exploration Agency (JAXA) (https://gportal.jaxa.jp/gpr/information/product). Tb36.5V is the most sensitive band for retrieving land surface information (Mcfarland et al., 1990). Since Tb for the microwave band is the product of ground temperature and emissivity, by using the Tb36.5V as the Quasi-temperature, the ratio of Tb between any lower frequencies and 36.5V can be considered as Quasi-emissivity (Qe) (Zhao et al., 2011). Qe can reflect the change in the dielectric constant caused by the change in the liquid water content in the soil. The AMSR2 F/T product was obtained through a parametric DFA (Wang et al., 2018). The DFA algorithm was developed based on the Fisher linear discriminant analysis method with Qe and Tb36.5V by the AMSR-E Tb and 5 cm in situ soil temperature data from the intensive soil temperature and moisture observation network at 46 stations in four countries distributed in the northern
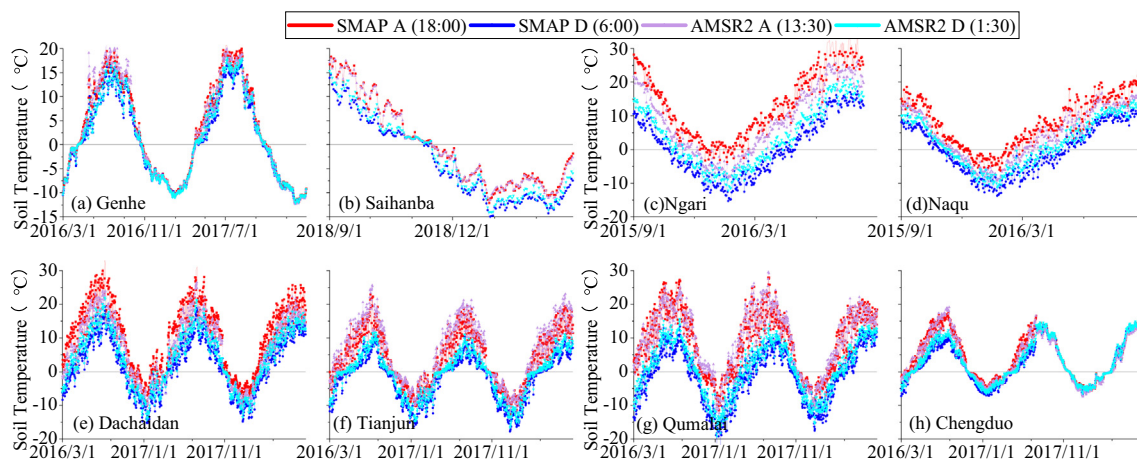
Fig. 2. Time series of in situ soil temperature at transit time of SMAP and AMSR2 in eight study areas.

hemisphere. The validation results with the same in situ measurement data show that the overall accuracy is 90.06%. DFA is defined as follows (Wang et al., 2018):

$$FTI\_A = -0.123 * Tb36.5V + 11.842 * (Tb18.7H/Tb36.5V) + 20.65 \tag{5}$$

$$FTI\_D = -0.209 * Tb36.5V + 9.384 * (Tb18.7H/Tb36.5V) + 43.697 \tag{6}$$

where FTI_A and FTI_D (Zhao et al., 2017) correspond to ascending (1:30 PM) and descending (1:30 AM) orbits, respectively, and Tb18.7H corresponds to Tb of 18.7 GHz at H-polarization. Finally, the F/T state of the land surface is obtained according to the following formula:

$$FTI < T, \text{ thaw} \tag{7}$$

$$FTI > T, \text{ freeze} \tag{8}$$

Here, T is set at 0. AMSR2 is a successor to AMSR-E with a sensor configuration similar to AMSR-E, such as orbit altitude, swath width, and equator crossing time. Therefore, we apply DFA directly to AMSR2 satellite data using the calibration equation developed by linear regression models with the coefficient of determination of 0.98 (Hu et al., 2019). The root-mean-square deviation (RMSD) from AMSR2 and AMSR-E ranges from 4.14 K to 4.57 K and mean bias ranges from 0.33 K to 2.64 K after intercalibration (Hu et al., 2019). The calibration equation between AMSR2 and AMSR-E is as follows (Hu et al., 2019):

$$Tb\_AE\_18.7H = 1.0189 * Tb\_A2\_18.7H - 5.2717 \tag{9}$$

$$Tb\_AE\_36.5V = 1.0135 * Tb\_A2\_36.5V - 6.3914 \tag{10}$$

where Tb_AE_18.7H (Tb_AE_36.5V) and Tb_A2_18.7H (Tb_A2_36.5H) correspond to AMSR-E Tb18.7H (36.5V) and AMSR2 Tb18.7H (36.5V), respectively. Finally, we used the DFA and AMSR2 L3 level Tb to obtain the AMSR2 F/T product.

2.2.3. MEaSUREs F/T products

MEaSUREs F/T product (version 4), based on MSTA and Tb36.5V can reflect the dynamic change of the dielectric constant when F/T occurs to detect F/T of land surface. The MEaSUREs F/T product used in this study was downloaded from National Snow and Ice Data Center (NSIDC). MSTA used empirical linear regression between Tb36.5V and ERA-interim surface air temperature (SAT) data to define the threshold of F/T for each pixel. The threshold for descending (AM) and ascending (PM) were determined by using the daily minimum SAT and the maximum SAT, respectively. In the case of pixel by pixel linear regression, SATs close to 0 °C were more heavily weighted based on cosine functions in the range −60.0 °C to 30.0 °C. MEaSUREs F/T product contain F/T data obtained by SMMR-SSM/I-SSMIS (1979 to 2017) and AMSR-

E/AMSR2 (2002 to 2017). Here, in order to compare the F/T products obtained from same satellite Tb data, we chose the MEaSUREs F/T products obtained from AMSR2 Tb.

We evaluated the performances of the SMAP, AMSR2 and MEaSUREs F/T products in ascending and descending orbits and then analyzed the main impact factors of these algorithms.

2.3. Evaluation metrics

The F/T classification accuracy was evaluated by the following three indices (Kou et al., 2017):

$$F\_right = FF/(FF+FT) * 100\% \tag{11}$$

$$T\_right = TT/(TT + TF) * 100\% \tag{12}$$

$$Total\_right = (FF + TT)/(FF + FT + TF + TT) * 100\% \tag{13}$$

where FF and TT represent the correctly classified numbers of frozen soil and thawed soil, respectively. FT and TF represent incorrectly classified numbers of frozen soil and thawed soil, respectively. Eqs. (11), (12) and (13) represent freeze accuracy, thaw accuracy, and overall accuracy, respectively. The in situ F/T state is defined by the temperature data corresponding to overpassing time of SMAP and AMSR2 when the soil (air) temperature is > 0 °C for the thawed state, and otherwise for the frozen state.

3. Results

3.1. Consistency in the F/T product and in situ data

Fig. 2 shows the in situ soil temperature of 5 cm at 6 a.m., 13:30 p.m., 18:00 p.m. and 1:30 a.m., corresponding to descending and ascending orbits of SMAP and AMSR2 in eight study areas, respectively. Except for the insignificant diurnal variation of soil temperature in Genhe and Chengduo study areas, the diurnal variation of soil temperature can be seen in other study areas. There was little difference between 13:30 and 18:00, 01:30 and 06:00 in Saihanba, Dachaidan, Tianjun and Qumalai. It can be seen that in the Ngari and Naqu study areas, there was a significant difference in the time of F/T transition between SMAP and AMSR2, which contribute to many days of daily F/T cycles and difficulties to F/T monitoring. By analyzing the differences in performance of the F/T product in the Ngari and Naqu study areas with additional days of daily F/T cycles, the advantages and limitations of F/T algorithms of SMAP, AMSR2, and MEaSUREs can be found. Here, "A" and "D" in Fig. 2 mean the ascending and descending orbits, respectively.

Figs. 3–6 show the time series of SMAP F/T flags, AMSR2 F/T flags,
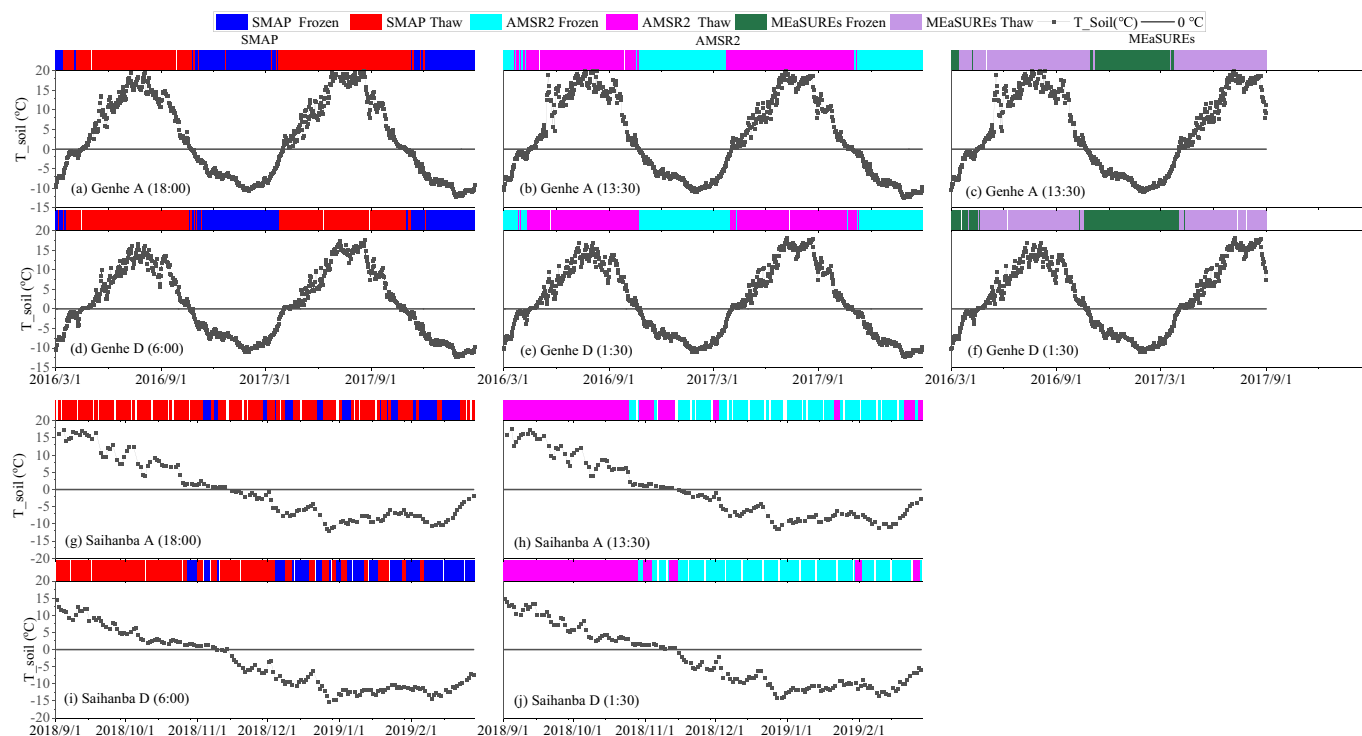
Fig. 3. Time series of SMAP F/T flags, AMSR2 F/T flags, MEaSUREs F/T flags and in situ soil temperature for Genhe ((a)–(f)) during March 2016 to February 2018 and Saihanba ((g)–(j)) during September 2018 to February 2019. (For interpretation of the references to color in this figure, the reader is referred to the web version of this article.)

MEaSUREs F/T flags and in situ soil temperatures at descending and ascending orbits in eight study areas. The bars above the plot are the F/T state detected by SMAP, AMSR2 and MEaSUREs, where red/pink/lilac, blue/cyan/dark green and white represent thawed, frozen and missing data, respectively. Additionally, the solid black line is the 0 °C temperature line. The time period for the areas varies depending on the availability of measurement data in each region. To ensure the comparability of the results among F/T products, the data were
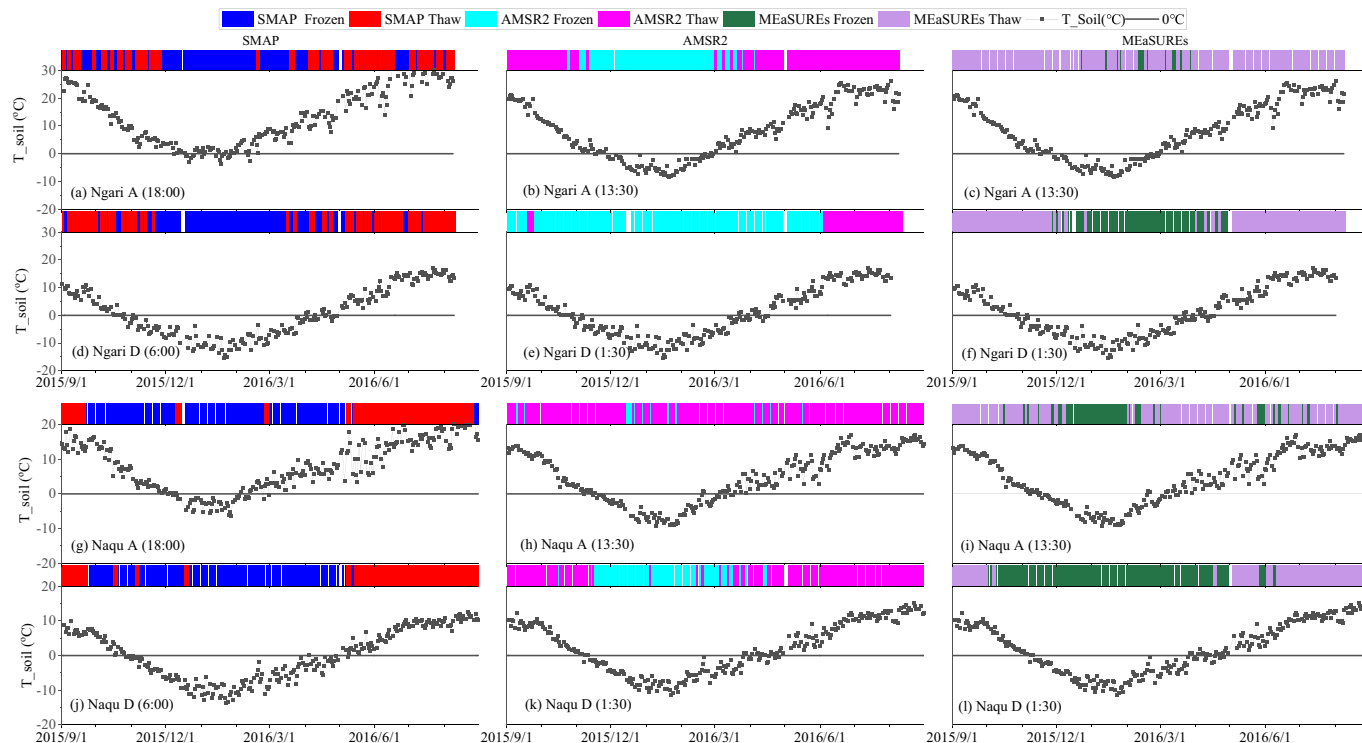

Fig. 4. Time series of SMAP F/T flags, AMSR2 F/T flags, MEaSUREs F/T flags and in situ soil temperature for Ngari ((a)–(f)) and Naqu ((g)–(l)) from September 2015 to August 2016. (For interpretation of the references to color in this figure, the reader is referred to the web version of this article.)
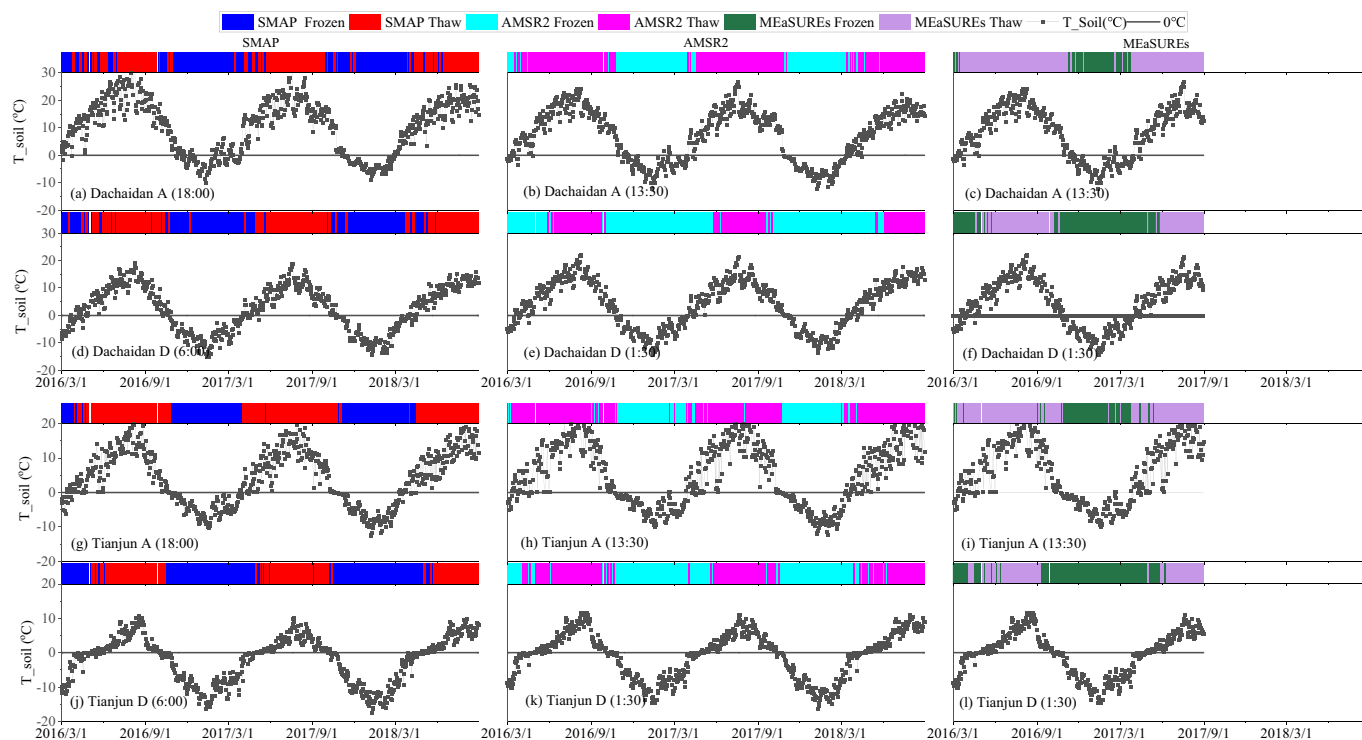
Fig. 5. Time series of SMAP F/T flags, AMSR2 F/T flags, MEaSUREs F/T flags and in situ soil temperature for Dachaidan ((a)–(f)) and Tianjun ((g)–(l)) from March 2016 to August 2018. (For interpretation of the references to color in this figure, the reader is referred to the web version of this article.)

preprocessed to ensure that F/T products and the in situ data had the same data records. The MEaSUREs F/T product was only updated until 2017, so there were no results in the Saihanba study area.

According to Figs. 3 and 6, the thawing times detected by the SMAP, AMSR2 and MEaSUREs F/T products are earlier than that detected by in situ soil temperature at Genhe and Chengduo (ascending orbits in 2018). Genhe belongs to a cold and humid temperate forest climate and a continental monsoon climate located in the humid and semi-humid zone, which has obvious F/T cycle characteristics. According to previous studies on the distribution characteristics of snow cover in China,
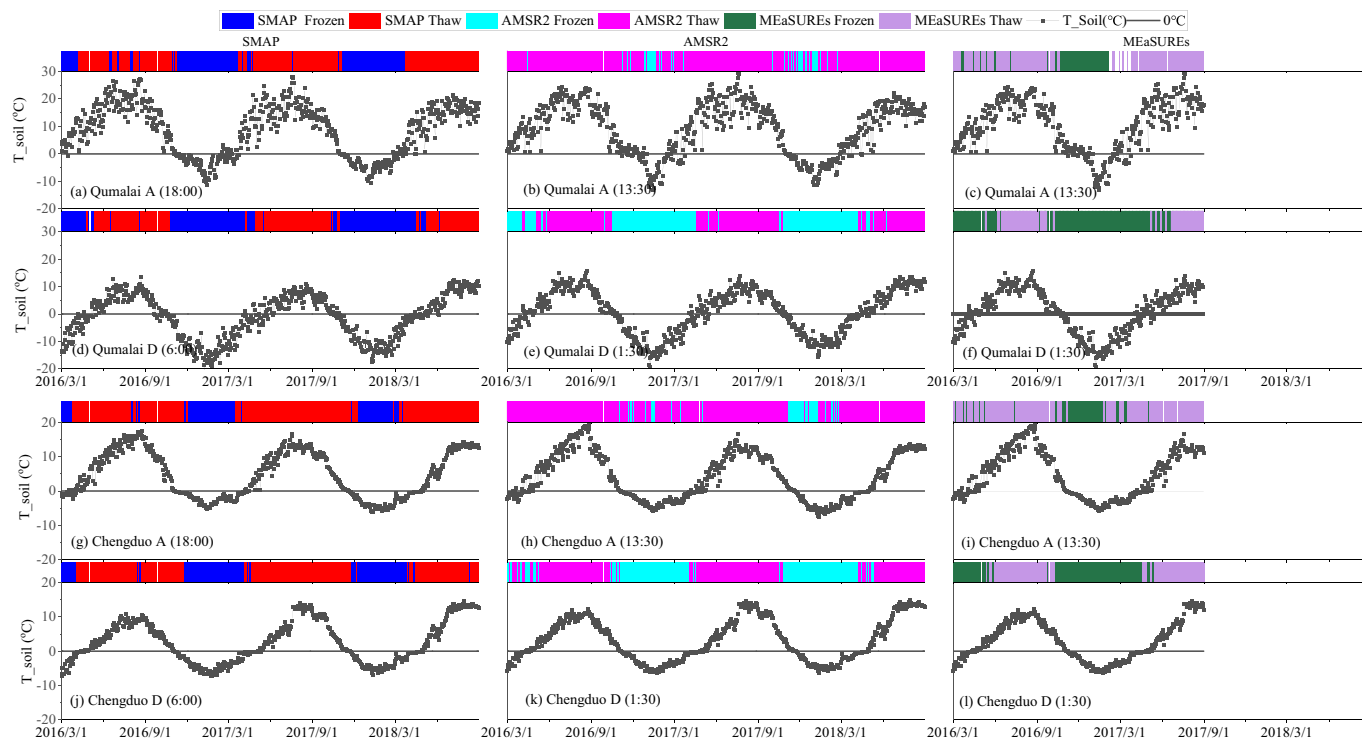

Fig. 6. Time series of SMAP F/T flags, AMSR2 F/T flags, MEaSUREs F/T flags and in situ soil temperature for Qumalai ((a)–(f)) and Chengduo ((g)–(l)) from March 2016 to August 2018. (For interpretation of the references to color in this figure, the reader is referred to the web version of this article.)

the Genhe study area belongs to a stable snow cover area whose annual snow cover days are generally > 90 days (Liu and Chen, 2011; Zhang and Zhong, 2014). Similarly, with the snow depth data from the snow depth automatic observatory dataset at Chengduo, there was continuous snow cover from February to March of 2018. The thawing time detected by satellites in spring is affected by the melting of snow, which generally occurred earlier than thawing at the 5-cm soil depth (Derksen et al., 2017; Du et al., 2015; Roy et al., 2015). This may be the main reason that both satellite F/T products show the early detection of thawing time in Genhe and Chengduo (2017 and 2018). Notably, only Saihanba has short observation data from September 2018 to March 2019, since the soil temperature and soil moisture observation network data were obtained since the end of August 2018. SMAP F/T products at Saihanba failed to detect frozen soil due to its misclassification of frozen soil when the soil temperature was stable at −10 °C in January, and this phenomenon is especially obvious during ascending orbits. The freezing time of the AMSR2 F/T product is consistent with the data measured at Saihanba, and the number of surface states misclassified as thawed soil is far less than those of the SMAP F/T product in January and February. This may be related to the Saihanba soil texture in North China, since the soil storage capacity of the Saihanba area is relatively poor due to high sand content (~70%) (Li et al., 2019; Wang et al., 2017b; Wang et al., 2017c) and the semi-arid and semi-humid climate. The NPR variation range is small in the sandy soil and semi-arid climate, and the NPR algorithm of SMAP failed to detect the F/T status.

In Figs. 4 and 5, the SMAP, AMSR2 and MEaSUREs F/T flags in the Ngali, Naqu and Dachaidan study areas show poor consistency with that of the soil temperature response. The corresponding annual thaw time of the SMAP and AMSR2 F/T products is shorter than that of the 5 cm soil temperature. In the Ngari, Naqu, and Dachaidan study areas, SMAP detected a large amount of thawed soil as frozen soil in spring because there is no significant increase in soil moisture as thawing occurs. The thawed surface from September to early October 2015 and April to May 2016 were all classified as a frozen surface by AMSR2 at Ngari during the descending orbit because of the combination of low soil moisture (high emissivity) due to arid climates and low temperatures at the descending orbit (1:30 AM), for similar radiation characteristics with frozen soil. At the end of July 2016, when the soil temperature reached 30 °C, SMAP also detected frozen surfaces in the Ngari area due to a sudden decrease in soil moisture caused by the soil temperature increase after precipitation. There is no such phenomenon in Ngari for AMSR2, possibly because the Tb36.5V used in DFA has a high correlation with surface temperature (Mcfarland et al., 1990), and such misclassification can be avoided according to the response of Tb36.5V to surface temperature. There are large differences in the duration of annual frozen soil according to the in situ soil temperatures corresponding to the overpass times of satellite ascending and descending orbits (Fig. 2), which contribute to many days of daily F/T cycles. The long duration of the daily F/T cycle may introduce difficulties in F/T monitoring. Moreover, these three study areas mainly comprise sandy soil with poor storage capacities. The NPR factor used by SMAP may be more sensitive to water changes (Rautiainen et al., 2014; Roy et al., 2015), and as a result, SMAP cannot detect soil F/T conversion in time over the Ngari, Naqu, and Dachaidan study areas due to the small amount of soil phase transition water content. For AMSR2, F/T could normally be distinguished between frozen soil with low temperature and high emissivity and thawed soil with high temperature and low emissivity. However, in the Ngari, Naqu and Dachaidan study areas, the surface emissivity was always high when the F/T conversion occurred due to small soil moisture changes.

According to Figs. 5 and 6, we found that the thawing times detected by both SMAP and AMSR2 are similar to the in situ soil temperature in the Tianjun and Qumalai areas, although the thawing times of the two F/T products detected in the Qumalai area were slightly later than the in situ soil temperature. According to the snow depth data, the snow cover days are all < 60 days, and the snow depth is < 5 cm in

most cases, with discontinuous snow cover over the two areas. In addition, snow melting has little effect on spring thaw detection over the Tianjun and Qumalai areas. Furthermore, the consistency in the freezing times detected by the two F/T products and in situ 5-cm depth soil temperature is good.

Overall, we found that the thaw state was detected by SMAP after the surface froze in December over Genhe and Saihanba. However, in the Qumalai, Tianjun, and Chengduo areas, no such phenomena occurred, which was because the difference in NPR thawing and freezing reference values in the Genhe and Saihanba areas is small, but this difference was great in the Qumalai, Tianjun, and Chengduo areas. This result indicated that the difference in NPR thawing and freezing reference values may affect the precision of the SMAP F/T product.

The MEaSUREs F/T product detected the thawing time that was earlier than that of soil temperature, and the annual thaw days were longer than that of 5 cm soil over ascending orbits in eight study areas. Conversely, the annual thaw days of the MEaSUREs F/T product during the descending orbits were shorter than that of 5 cm of soil, with early freezing in autumn and late thawing in spring. This was related to the ERA-interim data used by MEaSUREs. The time corresponding to the daily maximum temperature and minimum temperature of the SAT may not correspond to the transit time of the AMSR2 satellite. The daily minimum SAT may be lower than the soil temperature of 5 cm at 1:30, which would lead to the overestimation of the frozen state in descending orbits. The daily maximum SAT may be higher than the soil temperature of 5 cm at 13:30, resulting in an overestimation of the thawed state in ascending orbits.

3.2. F/T product validation results

To evaluate the seasonal performance of F/T products in different seasons, the validation work was divided into a soil freezing period (from fall to winter) and a soil thawing period (from spring to summer). Subsequent validation and analysis were carried out for these two periods.

3.2.1. Evaluation of F/T products in the freezing period

Fig. 7 shows the accuracies of the F/T products during the freezing periods when the soil transformed from thawed to frozen. The frozen soil was detected well by SMAP, AMSR2 and MEaSUREs in descending orbits in all areas (F_right > 80%, except for the poor accuracy of the SMAP in the Saihanba study area (~60%) and MEaSUREs in the Ngari study area (75%)). The freeze accuracy of AMSR2 and MEaSUREs in most areas is higher than that of SMAP, and the thaw accuracy of SMAP is higher than that of AMSR2 and MEaSUREs in the descending orbits. This finding indicated that in the freezing period, the surface freezing state may be detected by AMSR2 and MEaSUREs before SMAP, which is related to the weaker penetration of the AMSR2 (Ka-band and Ku-band) and MEaSUREs (Ka-band) than SMAP (L-band). The different thaw accuracies of SMAP and AMSR2 mainly occurred in the Ngari, Naqu and Dachaidan study areas influenced by the arid climate, where soil temperature decreased but soil moisture did not change significantly when freezing occurred. The change in the dielectric constant caused by changes in soil moisture is the main basis for SMAP and part of the basis for AMSR2 to detect F/T signals. MEaSUREs had a low thaw accuracy (< 60%) in most of the study areas during descending orbits because the penetration depth of Tb36.5V was the shallowest, and the minus temperature difference between the daily minimum temperature of ERA-interim and the 5 cm soil temperature would make MEaSUREs sensitive to the soil freezing in the shallower layer, and even lead to pre-freezing. Overall, the accuracy of the SMAP and AMSR2 F/T products in the descending orbit is higher than that in the ascending orbit because the soil F/T state (0–1 cm) corresponding to the descending orbit in the freezing period is more consistent with that of the 5 cm soil due to re-freezing of the top surface in descending. Another reason is that the intra-day thawing may occur during the ascending orbit of the
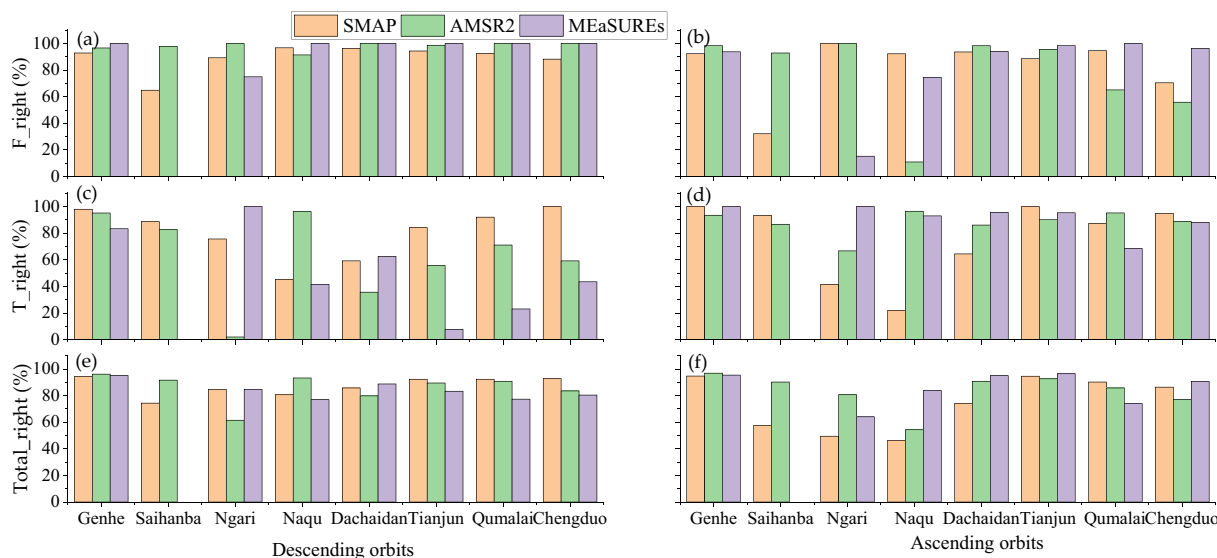
Fig. 7. Freeze accuracy ((a), (b)), thaw accuracy ((c), (d)), and overall accuracy ((e), (f)) for the study area over descending ((a), (c), (e)) and ascending ((b), (d), (f)) orbits during the freezing period.

0–1 cm depth of soil. This has a significant impact on the detection of F/T (Williamson et al., 2018) when the F/T state of 0–1 cm may be inconsistent with that of 5 cm soil. The overall accuracy of MEaSUREs F/T product is higher in ascending orbits.

In addition, the misclassification of thawed and frozen surface for SMAP, AMSR2 and MEaSUREs during the freezing periods is assessed according to the method of Derksen et al. (2017). The results are shown in Table 2. In Genhe, Saihanba, Tianjun and Chengduo study areas, more frozen soil was misclassified by SMAP (SMAP identified thawed soil and in situ measurements indicated frozen soil). This may mean that SMAP were more or less time-delayed in detecting a completely frozen surface over these areas during freezing periods. Tianjun and Chengduo were affected by the slight increase in soil moisture caused by snowfall and quick snowmelt in the early freezing periods, leading to the thawed soil being retrieved by SMAP. SMAP incorrectly retrieved frozen flags (SMAP identified frozen soil and in situ measurements indicated thawed soil) in the Ngari, Naqu, Dachaidan and Qumalai (ascending) areas, which may be affected by fluctuations in soil moisture caused by summer precipitation (Kou et al., 2017). Additionally, the Ngari, Naqu and Dachaidan areas contain water bodies, which may affect the F/T detection (Kim et al., 2017). AMSR2 misclassified frozen soil (especially ascending) in the Naqu area and thawed soil in the Saihanba, Ngari and Dachaidan areas, while it was found that the AMSR2 F/T classification results had extreme phenomena. That is, the surface F/T states were determined as frozen or thawed in the whole year because of the same equation and threshold used. DFA ignored the characteristics of surface emissivity and temperature of F/T soil in different climatic types, land cover and terrain heterogeneity.

3.2.2. Evaluation of F/T products in the thawing period

Fig. 8 shows the accuracies of SMAP, AMSR2 and MEaSUREs in the thawing period when the soil transformed from frozen to thawed. Table 3 shows the statistical misclassification of frozen and thawed soils by the SMAP, AMSR2 and MEaSUREs F/T products in the thawing period. Because of the short observation time in the Saihanba area, the accuracy in the thawing period has not yet been validated. The SMAP F/T product has a better freeze accuracy in the ascending period and better thaw accuracy in the descending period in relation to the in situ data at a 5 cm depth. The SMAP L-band is very sensitive to the water that can capture thawing signals from the first centimeter into the surface (Williamson et al., 2018) when the 5 cm depth soil is still frozen, leading to low thaw accuracy at Genhe and Chengduo (Table 3)

in ascending orbits. In addition, other study areas (Ngari, Naqu and Dachaidan in Table 3) are influenced by the arid climate where soil moisture had no significant change when the 5-cm depth soil is thawing. However, the overall accuracy of SMAP is better in the descending orbit due to the consistent F/T state between the uppermost surface and the 5-cm depth caused by the uppermost surface tending to refreeze (Derksen et al., 2017). According to Table 3, the misclassifications of AMSR2 and SMAP are relatively consistent. There are differences in the Naqu study area; however, the DFA method has extreme classification errors in the Naqu study area for failing to detect the frozen period in winter during ascending orbits due to little difference in emissivity and temperature when F/T occurred. In addition, SMAP showed more misclassification of thawed soil, while AMSR2 showed more misclassification of frozen soil in the Qumalai area during the ascending orbits because SMAP mistakenly detected frozen signals in summer due to rainfall, while the DFA method rarely made such mistakes with the aid of temperature factors. The MEaSUREs F/T product identified the thawed soil as frozen soil during the descending orbits, thus detecting a later thawing time than that of 5 cm soil. Instead, the MEaSUREs F/T products identified more thawed soil, which led to an early thawing time obtained during ascending orbits; moreover, the misjudgment of thawed soil in summer is serious in ascending orbits, especially in the QTP study area, which may be caused by the influence of summer snowfall.

Tables 4 and 5 show the overall accuracies of the SMAP, AMSR2 and MEaSUREs F/T products in ascending and descending orbits in relation to freezing and thawing periods. In addition to Saihanba, Ngari, Naqu, and Dachaidan, SMAP and AMSR2 exhibited little accuracy difference between ascending and descending orbits. The difference in the overall accuracy of SMAP and AMSR2 between descending and ascending orbits occurred in the Ngari, Naqu, and Dachaidan study areas. In these areas, there are great F/T differences between descending (6:00/ 1:30 AM) and ascending (6:00/1:30 PM) orbits as indicated by the soil moisture and temperature. However, the consistent F/T state occurred in the descending orbits, which was caused by the consistent frozen state, as indicated by small water changes during the F/T transition and low temperature. There is a great accuracy difference between ascending and descending orbits of MEaSUREs in QTP, which may be related to the large ERA-interim air temperature difference between overpass orbits, while a small difference occurs in the soil temperature.

Table 2

Performance metrics of the SMAP and AMSR2 F/T products compared with in situ soil temperature data for the freezing period in the eight study areas (Tsoil-F (Tsoil-T) means that a frozen (thawed) state is indicated by soil temperature). Fern green/calamine blue/cyan indicates the misclassification of frozen soil by the SMAP/AMSR2/MEaSUREs F/T products, while mango/orange/pink indicates the misclassification of thawed soil by the SMAP/AMSR2/MEaSUREs F/T products; N is the number of evaluation data for each site.

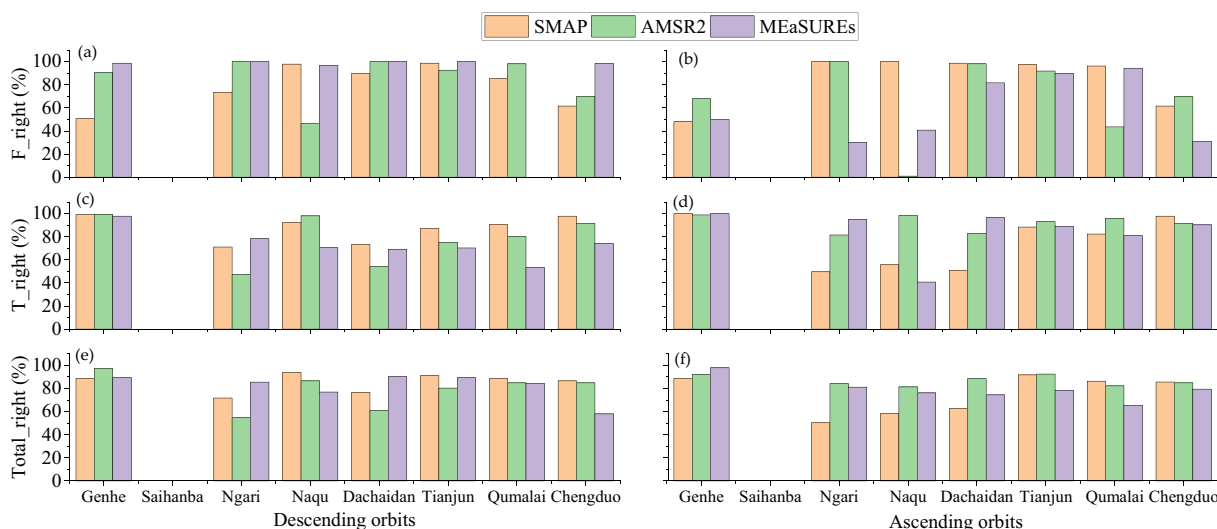| In situ areas	F/T product	Morning (Nighttime) orbits			Afternoon (Daytime) orbits		
		Tsoil-F	Tsoil-T	N	Tsoil-F	Tsoil-T	N
Genhe	SMAP-F	65.38	0.59	338	63.79	0	359
	SMAP-T	5.03	28.99	338	5.29	30.92	359
	PDFA-F	67.46	1.48	338	68.8	1.95	359
	PDFA-T	2.37	28.7	338	1.11	28.13	359
Saihanba	SMAP-F	39.1	4.49	156	18.75	2.78	144
	SMAP-T	21.15	35.26	156	39.58	38.89	144
	PDFA-F	57.69	7.05	156	54.17	5.56	144
	PDFA-T	1.28	33.97	156	4.17	36.11	144
Ngari	SMAP-F	60	8	125	13.76	50.46	109
	SMAP-T	7.2	24.8	125	0	35.78	109
	PDFA-F	60.8	38.4	125	42.2	19.27	109
	PDFA-T	0	0.8	125	0	38.53	109
Naqu	SMAP-F	66.67	17.04	135	32.14	50.89	112
	SMAP-T	2.22	14.07	135	2.68	14.29	112
	PDFA-F	55.56	1.48	135	5.36	1.79	112
	PDFA-T	5.19	37.78	135	43.75	49.11	112
Dachaidan	SMAP-F	69.03	11.57	268	30.41	23.99	296
	SMAP-T	2.61	16.79	268	2.03	42.58	296
	PDFA-F	68.66	20.15	268	38.51	8.45	296
	PDFA-T	0	11.19	268	0.68	52.36	296
Tianjun	SMAP-F	75.61	3.14	287	42.6	0	277
	SMAP-T	4.53	16.72	287	5.42	51.99	277
	PDFA-F	77.7	9.41	287	46.57	5.05	277
	PDFA-T	1.05	11.85	287	2.17	46.21	277
Qumalai	SMAP-F	70.34	1.9	263	38.55	7.64	275
	SMAP-T	5.7	22.05	263	2.18	51.64	275
	PDFA-F	68.44	9.13	263	20.36	3.27	275
	PDFA-T	0	22.43	263	10.91	65.45	275
Chengduo	SMAP-F	53.18	0	267	24.54	3.3	273
	SMAP-T	7.12	39.7	267	10.26	61.9	273
	PDFA-F	59.55	16.48	267	19.41	7.33	273
	PDFA-T	0	23.97	267	15.38	57.88	273

Fig. 8. Freeze accuracy ((a), (b)), thaw accuracy ((c), (d)), and overall accuracy ((e), (f)) for the study area over descending ((a), (c), (e)) and ascending ((b), (d), (f)) orbits during the thawing period.

Table 3
Performance metrics that correspond to those in Table 2 but for the thawing periods.

In situ areas	F/T product	Morning (Nighttime) orbits			Afternoon (Daytime) orbits		
		Tsoil-F	Tsoil-T	N	Tsoil-F	Tsoil-T	N
Genhe	SMAP-F	10.92	0.57	348	10.16	0	364
	SMAP-T	10.63	77.87	348	10.99	78.85	364
	PDFA-F	18.97	0.57	348	14.56	0.82	364
	PDFA-T	2.01	78.45	348	6.87	77.75	364
Ngari	SMAP-F	21.37	20.51	117	1.44	49.64	139
	SMAP-T	7.69	50.43	117	0	48.92	139
	PDFA-F	13.68	45.3	117	14.39	15.83	139
	PDFA-T	0	41.03	117	0	69.78	139
Naqu	SMAP-F	33.33	5.19	135	5.77	41.67	156
	SMAP-T	0.74	60.74	135	0	52.56	156
	PDFA-F	10.37	1.48	135	0	1.28	156
	PDFA-T	11.85	76.3	135	17.31	81.41	156
Dachaidan	SMAP-F	18.93	21.12	412	24.57	37.02	289
	SMAP-T	2.18	57.77	412	0.35	38.06	289
	PDFA-F	15.05	38.83	412	36.33	10.73	289
	PDFA-T	0	46.12	412	0.69	52.25	289
Tianjun	SMAP-F	33.79	8.39	441	37.94	7.09	282
	SMAP-T	0.45	57.37	441	1.06	53.9	282
	PDFA-F	28.12	17.23	441	36.17	4.26	282
	PDFA-T	2.27	52.38	441	3.19	56.38	282
Qumalai	SMAP-F	31.85	5.93	405	28.04	12.55	271
	SMAP-T	5.43	56.79	405	1.11	58.3	271
	PDFA-F	25.43	14.57	405	11.44	2.95	271
	PDFA-T	0.49	59.51	405	14.76	70.85	271
Chengduo	SMAP-F	20.63	1.46	412	33.46	0	272
	SMAP-T	12.86	65.05	412	18.01	48.53	272
	PDFA-F	21.36	5.83	412	10.66	0.74	272
	PDFA-T	9.22	63.59	412	45.59	43.01	272

3.2.3. Evaluation difference between soil and air temperatures for F/T products

A series of previous studies (Derksen et al., 2017; Roy et al., 2015; Roy et al., 2017a; Roy et al., 2017b) have shown that in the thawing period, the F/T detected by satellites was vulnerable to the increase in moisture caused by snow melt. F/T products would be more likely to better agree with air temperature. However, most of the study areas in these studies are located in mid-high latitudes with persistent snow cover from winter to spring. The aim of this section is to determine the similarities and differences between air temperature and soil temperature in evaluation of F/T products at low and middle latitudes. We compared and separately analyzed the performances of SMAP, AMSR2 and MEaSUREs F/T products using 5 cm depth soil temperature and 2 m air temperature data observed in the Dachaidan, Tianjun, Qumalai, and Chengduo areas. The reason for selecting these four areas is that only these four areas have both measurements of soil temperature and air temperature.

Fig. 9 shows the freeze and thaw accuracies of the Dachaidan, Tianjun, Qumalai, and Chengduo study areas during the thawing period. The difference in thaw accuracies between the air temperature used and soil temperature used was 4.19%, 9.75% and 12.12% of SMAP, AMSR2, and MEaSUREs over descending orbits, respectively. The T_right detected by the three F/T products were more consistent with the air temperature in descending orbits. Moreover, the MEaSUREs F/T product that used the single channel of Tb36.5 V had the largest difference of T_right between air and soil temperature, while AMSR2 exhibited the second largest difference, and SMAP exhibited the smallest. This indicates that the three F/T products had a delayed response to 5 cm soil thawing during the thawing periods, and SMAP with the longest penetration had the lowest latency, while MEaSUREs with the shallowest penetration and has been calibrated to air temperature had the highest latency. The difference in thaw accuracies between the air temperature used and soil temperature used was −1.13% of the three F/T products over ascending orbits. This indicates that the three F/T products are more consistent with 5 cm soil temperature over ascending orbits.

Overall, the accuracy of F/T classification obtained by soil temperature as validation data is higher than that obtained by air

Table 4
The overall accuracies (%) of SMAP, AMSR2 and MEaSUREs F/T products in eight study areas during freezing and thawing periods over descending orbits.

F/T period	F/T product	Genhe	Saihanba	Ngari	Naqu	Dachaidan	Tianjun	Qumalai	Chengduo
Freezing period	SMAP	94.38	74.36	84.8	80.74	85.82	92.33	92.4	92.88
	AMSR2	96.15	91.67	61.6	93.33	79.85	89.55	90.87	83.52
	MEaSUREs	95.29	/	84.8	77.04	88.81	83.33	77.44	80.45
Thawing period	SMAP	89.01	/	50.36	58.33	62.63	91.84	86.34	85.68
	AMSR2	92.31	/	84.17	81.41	88.58	92.55	82.29	84.95
	MEaSUREs	97.99	/	81.2	76.3	74.45	78.57	65.56	79.56

Table 5
The overall accuracies that correspond to those in Table 4 but for ascending orbits.

F/T period	F/T product	Genhe	Saihanba	Ngari	Naqu	Dachaidan	Tianjun	Qumalai	Chengduo
Freezing period	SMAP	94.71	57.64	49.54	46.43	73.99	94.58	90.18	86.45
	AMSR2	96.94	90.28	80.73	54.46	90.88	92.78	85.82	77.29
	MEaSUREs	95.53	/	64.22	83.93	95.16	96.49	73.99	90.7
Thawing period	SMAP	88.79	/	71.79	94.07	76.7	91.16	88.64	86.68
	AMSR2	97.41	/	54.7	86.67	61.17	80.5	84.94	84.95
	MEaSUREs	89.29	/	85.61	76.92	90.34	89.36	84.44	58.09

temperature due to the penetration depth of SMAP and AMSR2. These findings indicated that in the study areas located in the low and middle latitudes with low snow cover and grasslands, SMAP and AMSR2 F/T products are more likely to reflect the surface soil F/T state, rather than the F/T state indicated by air temperature. MEaSUREs had a better consistency with the air temperature with calibrated to air temperature and shorter penetration depth of 36.5 GHz.

4. Discussion

4.1. Influence of soil moisture and temperature on the two algorithms

According to the validation results, the accuracies of the SMAP and AMSR2 F/T products in the Ngari, Naqu and Dachaidan areas with cold and arid and cold and semi-arid climate types is lower than 80%, and the performances of the two products in these areas greatly differs. In these study areas, the change in soil moisture is very small when the F/T transition occurs, but the soil temperature between the satellite ascending and descending orbits varies greatly over time, which may affect the applicability of the algorithm. To analyze the influence of soil moisture and temperature along different climate types on F/T monitoring, the sensitivity of the SMAP and AMSR2 F/T algorithms to soil moisture and temperature and the specific effects of temperature and soil moisture on the accuracy of the algorithm are analyzed here.

4.1.1. Sensitivity of the algorithms to soil moisture and temperature

SMAP detects F/T according to the NPR seasonal change caused by the dielectric constant, and the AMSR2 algorithm detects F/T based on emissivity and temperature changes. To distinguish the sensitivity of the two algorithms to the ground temperature and dielectric constant, the relationship between NPR and DFA and soil dielectric constant and temperature based on simulation are shown here. In the simulation process, the combined model for cold land developed by Zhao et al. (2011) was used to simulate the Tb of the F/T surface in the case of bare soil, forest and snow cover at 18.7 and 36.5 GHz respectively. Based on the combined model for cold land, the L-band dielectric model of F/T soil developed by Mironov et al. (2015) was used to replace the

dielectric model of Zhang et al. (2003a) in the combined model for cold land, and the brightness temperature of the L-band was simulated under the same conditions as 18.7 and 36.5 GHz in this work.

Fig. 10 shows the sensitivities of NPR and DFA to soil dielectric constants and temperature from the model simulation. The R^2 between NPR and dielectric constants is higher than that between ground temperatures because NPR is actually obtained by the ratio of L-band Tb, which cancels out the effect of temperature on NPR. The NPR reflects the change in dielectric constants caused by water change. The DFA has a higher R^2 with ground temperature than that with soil dielectric constants due to Tb36.5V being considerably sensitive to land surface temperature (Mcfarland et al., 1990; Parinussa et al., 2011). This leads to the DFA is sensitive to changes of both ground temperature and dielectric constant, while being more susceptible to ground temperature changes in F/T monitoring. According to the above analysis, the SMAP F/T detection algorithm mainly responds to changes in soil dielectric constants, namely, the change in soil moisture, while the AMSR2 F/T detection algorithm is mainly affected by changes in ground temperature.

4.1.2. Effects of soil moisture and temperature on the F/T algorithm

First, the error histogram of each study area is analyzed in Fig. 11, and the incorrect ground temperature classification is mainly distributed between −10 °C and 10 °C. Here, we did not consider the impacts of the station number and distribution differences over different study areas. In the Ngari and Naqu study areas, due to little change in soil moisture during the F/T transition caused by an arid climate and precipitation events in summer, the incorrectly classified data of SMAP and AMSR2 are distributed over a wide temperature range (−10 °C ~30 °C). Fig. 12 shows the variation in soil moisture with temperature during the thawing and freezing periods in the eight study areas. According to Fig. 11, the range of the horizontal axes in Fig. 12 is constrained between −10 °C and 10 °C because the major F/T misclassification events occur in this interval. There was no significant difference in the soil moisture change in the overpass time of the SMAP and AMSR2 in the eight study areas, nor was there a significant difference between the ascending and descending orbits. In the freezing
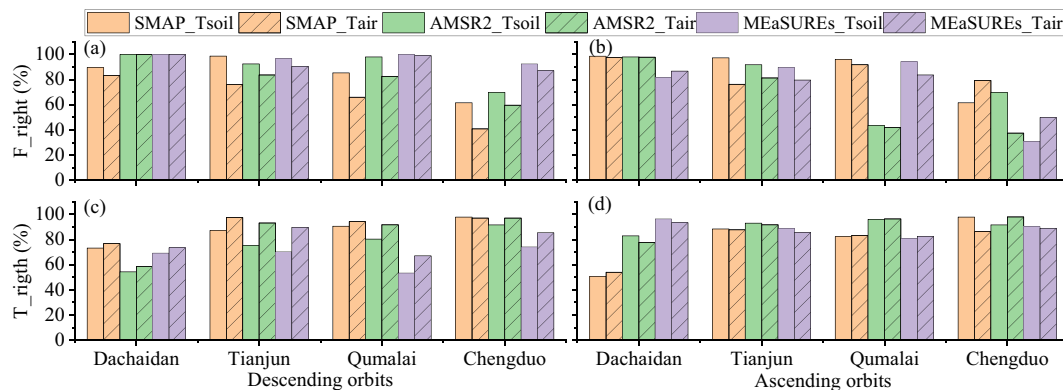

Fig. 9. The F/T discrimination accuracies in the Dachaidan, Tianjun, Qumalai, and Chengduo study area over descending (left) and ascending (right) orbits during the thawing period.
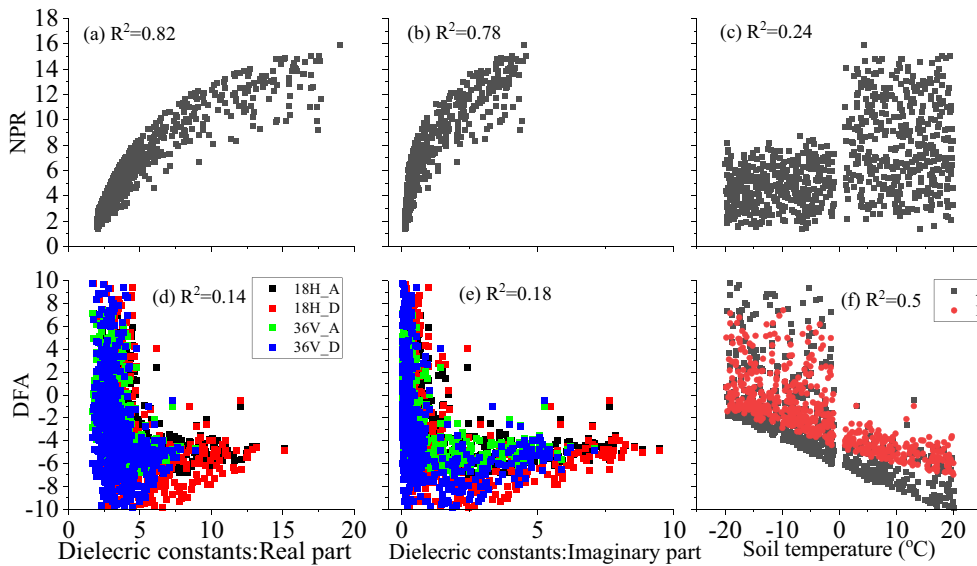
Fig. 10. Different sensitivities of soil dielectric constants and temperature to NPR (L-band) and DFA (Ka- and Ku-bands).

period, the soil moisture hardly changed and always remained at a lower value (0.05–0.1 m^3/m^3) during the process of soil temperature decline below 0 °C in the Ngari and Dachaidan areas, resulting in a frozen soil retrieval by SMAP when the soil temperature is higher than 0 °C. At the Naqu site, the soil moisture was reduced from relatively high (0.03 m^3/m^3) to low (0.01 m^3/m^3) when the temperature was higher than 0 °C, which leads to earlier frozen time detection by SMAP during freezing periods. These results lead to a large difference between freeze and thaw accuracies (F_right-T_right ≈ 20%) for SMAP in the Ngari, Dachaidan and Naqu study areas. The amount of SMAP NPR that failed to capture soil freezing caused by soil moisture change is small (0.1 m^3/m^3) when the soil temperature decreases from 2 °C to −2 °C, resulting in the overestimation of thawed soil by SMAP at Saihanba. SMAP obtained good freeze and thaw accuracies for the 0.2 m^3/m^3 soil moisture change when the soil temperature decreased from 2 °C to −2 °C in the Genhe, Tianjun and Qumalai areas. In the thawing period, soil moisture changes from low (0.1 m^3/m^3) to high (0.4 m^3/m^3) before the soil temperature rises to 0 °C in the Genhe and Chengduo study

areas, leading to an earlier soil thawing time detected by SMAP. Therefore, the thaw accuracy of SMAP in these two areas is higher than the freeze accuracy (T_right-F_right ≈ 50%). SMAP failed to detect thawing because the soil moisture was stable at a low value with no significant change when the soil temperature increased in the Ngari, Naqu and Dachaidan study areas.

The above results indicate that the SMAP F/T detection algorithm can well detect soil F/T when the change in soil moisture during F/T conversion periods reached 0.2 m^3/m^3 or higher. Little change in soil moisture during the freezing or thawing periods (always at a low stable value) can lead to overestimation of frozen flags in the SMAP F/T products. SMAP NPR is very sensitive to changes in soil moisture. The NPR in the time series can reflect the change trend in soil moisture based on findings from approximately eight areas. However, the SMAP F/T detection algorithm, which used a fixed threshold of 0.5 to identify freezing and thawing, may lead to the underestimation of frozen flags when the change in soil moisture is small (0.1 m^3/m^3) during the freezing periods.
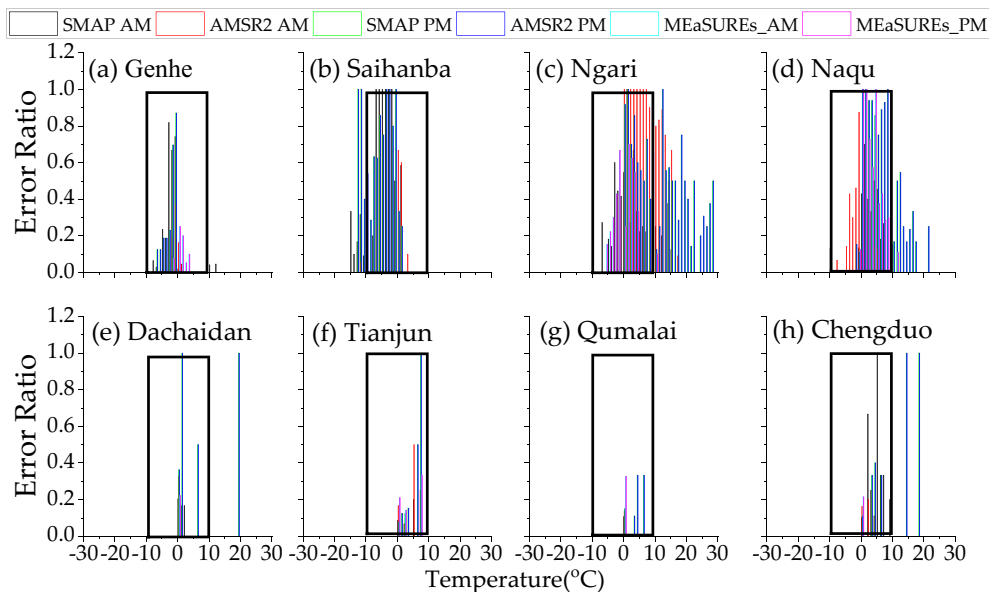

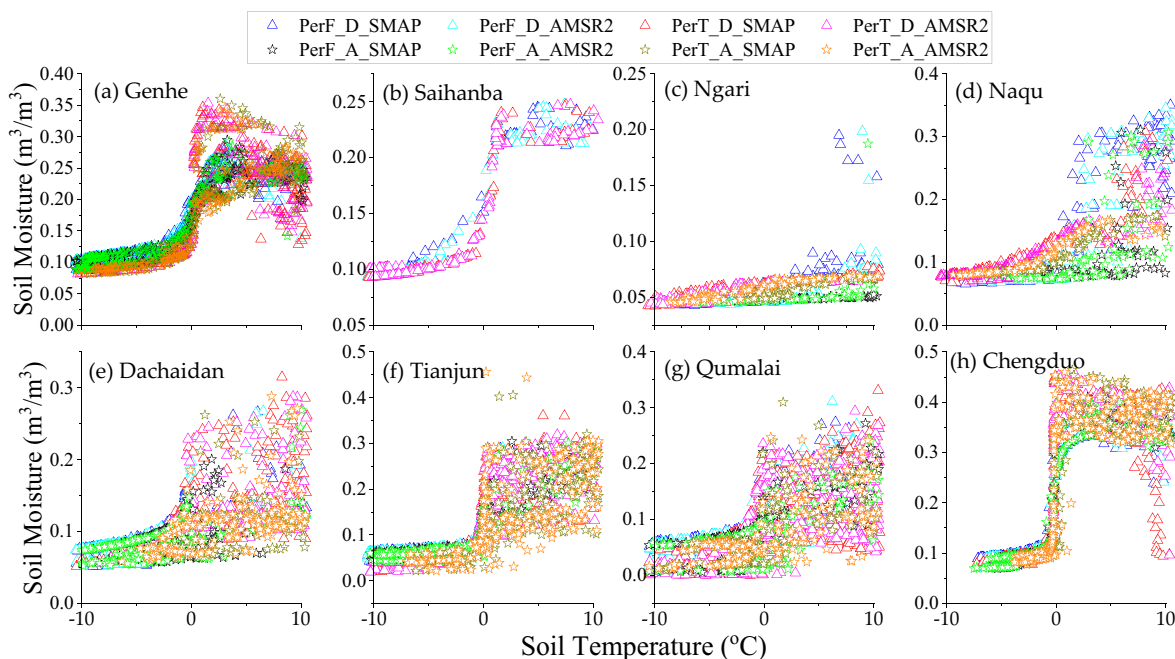**Fig. 11.** Histogram of the error ratio with temperature distribution.

Fig. 12. The variation in soil moisture with soil temperature in the Genhe (a), Saihanba (b), Ngari (c), Naqu (d), Dachaidan (e), Tianjun (f), Qumalai (g) and Chengduo (h) areas during the freezing periods and thawing periods. A and D represent ascending orbits and descending orbits, respectively. PerF and PerT represent the freezing period and thawing period, respectively.

4.2. The effect of snow cover on detected F/T

Previous studies (Derksen et al., 2017; Roy et al., 2015; Roy et al., 2017a; Roy et al., 2017b) have shown that the F/T retrieved by satellites is influenced by snow melt during thawing periods, which contributed to F/T products showing better agreement with air temperature than the 5-cm depth soil temperature. However, to determine whether snow cover always influences F/T detection or the circumstances under which snow cover affects F/T detection, we used in situ measurements at Chengduo from the snow depth dataset of the QTP to analyze the impact of snow cover on F/T detection. The reason for choosing this area is that the impact of more and less snow cover days on both detected F/T can be seen here. Fig. 13 shows the time series of snow cover, soil moisture, soil temperature, air temperature and F/T products at Chengduo during ascending orbits. The annual snow cover days in the Chengduo area from 2016 to 2018 vary from 17 to 97 with little thickness (< 25 cm), and the covering effect of the surface soil is not strongly similar to the snow in North America and Europe with a great thickness. The snow cover in Chengduo lasted for a short time and

melted quickly during 2016 and 2017, but a longer time in 2018 until the soil began to thaw.

In 2016 and 2017, the snow melted before the soil began to thaw when the soil remained frozen and the soil moisture was stable in a low value range, leading to the F/T detection algorithm of SMAP not being influenced by snow melting. However, with the snow cover in March 2016 and March 2017, AMSR2 classified the frozen surface as thawed when the air temperature was higher than 0 °C. This may be because during the AMSR2 ascending overpass (1:30 PM), due to being affected by higher snow humidity caused by an air temperature of > 0 °C, the detection algorithm of AMSR2 F/T, which is limited by the penetration depth of the Ka-band and Ku-band, may reflect the thawing signal of the snow layer or the top centimeter of soil. It is also possible that the increased TB36.5V that accompanied the snow melt would lead to the detection of the thawed soil. However, the misjudged frozen soil by MEaSUREs between March 2016 and March 2017 was less than that by AMSR2. This may be because although the MEaSUREs used the ERA-interim air temperature data to define the threshold for F/T determination, it used one-year time series data which can effectively reduce
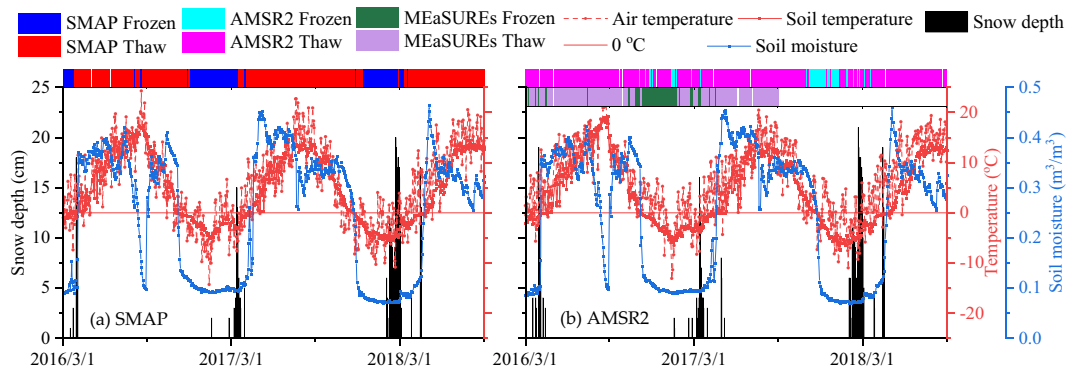

Fig. 13. In situ values of snow depth (black bar), soil moisture (blue solid line), soil temperature (red solid line), air temperature (red dotted line) and F/T product (bar above each plot) from March 2016 to August 2019 at overpass times for SMAP (a), AMSR2 and MEaSUREs (b) over Chengduo. (For interpretation of the references to colour in this figure legend, the reader is referred to the web version of this article.)

the impact of daily air temperature fluctuations on F/T determination. Both the SMAP and AMSR2 F/T products had a certain response to snow melting in March 2018 due to the increase of soil moisture. This indicates that the snow melting in spring would affect the response of SMAP and AMSR2 F/T products to ground F/T, but SMAP is not affected by winter snowmelt, while AMSR2 is affected by winter snowmelt, leading to misclassification of frozen soil. However, different from previous studies (Du et al., 2015; Roy et al., 2015), whose study areas were located in boreal forest areas with a long duration of snow cover days with close thawing time between snow and soil, for the middle and low latitude areas studied in this paper (Tianjun and Qumalai) where snow lasted for a short time and fast melting occurred with no snow cover over the thawing soil, the impact of snow melting on F/T products could be ignored.

4.3. Land parameter effects on F/T detection

The rough spatial resolutions of the SMAP, AMSR2 and MEaSUREs F/T products (~36 km for SMAP, 0.25° for AMSR2 and 25 km for MEaSUREs) with subpixel spatial heterogeneity would influence the assessment results. Thus, we analyzed the standard deviation of the digital elevation model (DEM) in the corresponding pixels of SMAP, AMSR2 and MEaSUREs and analyzed the relationship between the accuracies of F/T products and the elevation heterogeneities in the pixel. Simultaneously, the study areas are different in terms of soil texture because they have high clay content (Genhe and Tianjun) and high sand content areas (Saihanba, Ngari, Naqu and Dachaidan). We found that the difference in soil texture may also affect the detection accuracy of the F/T products. The sandy soil has a poor water storage ability, and through an analysis prior to soil moisture measurement, it is has been found to be an important factor in monitoring F/T; consequently, the relationship between sand content and F/T classification accuracy are analyzed. Both results are shown in Fig. 14. With increasing sand content, the F/T classification accuracies of SMAP, AMSR2 and MEaSUREs show a decreasing trend. The decreasing trend in SMAP is more obvious than that of AMSR2 and MEaSUREs because of the greater sensitivity of the SMAP F/T detection algorithm to water change. With the increase in the standard deviation of the DEM in the pixel, the accuracies of SAMP, AMSR2 and MEaSUREs show a downward trend, and the downward trend is similar because the satellite pixels of SMAP and AMSR2 are both rough.

Table 6 shows the number of false alarm mitigations and records of all SMAP data of SMAP F/T products corresponding to ascending and descending orbits in each study area. It can be seen that SMAP performs more false alarm mitigation operations in the Genghe, Ngari and Dachaidan study areas. Although the SMAP F/T algorithm included the step of false alarm mitigation, the frozen surface could still be detected in the QTP region during the summer. This may have been caused by the use of the daily AMSR (AMSR-E and AMSR2 Tb36.5V) F/T global

record data (2002–2015) in masking the "never frozen" and "never thawed" area in the process of false flag mitigation. The AMSR F/T global record is detected by daily Tb36.5V and reanalysis air temperature data from the National Centers for Environmental Prediction and National Center for Atmospheric Research (NECP-NCAR). Mao et al. (2010) evaluated the performances of ECMWF reanalysis (ERA-40), Japanese 25-year reanalysis (JRA-25), and NCEP/Department of Energy Global reanalysis 2 (NECP-2) in China, and the results showed that NECP-2 had the worst performance, especially in the QTP area, which has a complex terrain, and the data performance in summer was worse than that in winter. Cui and Wang (2009) found that the NECP-1 and NECP-2 reanalysis data are highly uncertain in the QTP. The differences between ERA-interim data and ground observation data in the QTP were also analyzed and compared, and the results showed that the ERA-interim data had a better applicability in the QTP area (Chen et al., 2019), while a large difference was found between the ERA-interim data and NECP-R2 data (MIing et al., 2019). All these analyses show that the performance of the reanalysis data in the QTP area is largely uncertain, which may have a negative influence on the SMAP retrieved F/T. Both the SMAP and AMSR2 F/T products had delayed detections of spring thawing time in the QTP area. The QTP is the plateau with the largest area, highest altitude, most diverse topography and most uneven surface in the world. The special geographical location and ecological climate environment of the QTP differentiate it from the Genhe and Saihanba study areas. The SMAP and AMSR2 F/T algorithms use 0.5 and 0 fixed thresholds to retrieve F/T, respectively, leading to different performances of the two algorithms in different study areas. It is very important to set the F/T classification threshold according to the characteristics of the study area.

It is well known that the L-band of SMAP has a deeper penetration than AMSR2. Furthermore, the FT classification of SMAP should theoretically be more consistent with the F/T state of 5 cm soil, but from our validation, there is little difference between SMAP and AMSR2 in response to the F/T state of 5 cm soil in the nonarid region. The results are the same as those in the work of Wang et al. (2018). It might have been caused by the calibration of the AMSR2 F/T algorithm with soil temperature data of 5 cm, minimizing the effects of the shorter penetration of the Ku- and Ka-band on the AMSR2 F/T classification. At the same time, in the freezing period, AMSR2 has a better penetration of frozen soil than wet soil, and it can detect the F/T state of 5 cm soil. Therefore, in the freezing periods, AMSR2 showed little difference from SMAP on overall accuracy. In addition, the dielectric constant of the soil increased when thaw occurred, and it is easier to identify the F/T with the frequencies difference of Tb18.7H and Tb36.5V. The SMAP F/T algorithm is also sensitive to soil F/T with NPR as the indicator. Both SMAP and AMSR2 first reflect the top layer thawing during the thawing period, resulting in a similar performance. Because the penetration depth of Tb36.5 V and SAT is used as auxiliary data, the depth of F/T information indicated by MEaSUREs is shallower than that of SMAP and AMSR2. In addition, regardless of whether SMAP (L-band), AMSR2 (Ku- and Ka-band), or MEaSUREs (Ka-band) is considered, the approach is unable to accurately detect F/T in areas with a complex land cover and terrain due to the coarse spatial resolution of passive microwave remote sensing.

The F/T detected by microwave remote sensing with a certain penetration depth should theoretically derive mainly from the soil, so it is necessary to use soil temperature data to validate F/T products. There are 9, 7, 3 and 16 sites sparsely distributed within the SMAP and AMSR2 pixels in Genhe, Saihanba, Ngari and Naqu study areas, respectively. Considering the number of sites and the sparse distribution within the SMAP and AMSR2 pixels, the average soil temperature of sites would be a better choice to represent the spatial average soil temperature of satellite pixels. However, Dachaidan, Tianjun, Qumalai and Chengduo study areas contain only one site in a grid of the satellite scale, but these data provide results from extended space, diverse land cover (bare land and grassland), climate types (inland plateau desert,
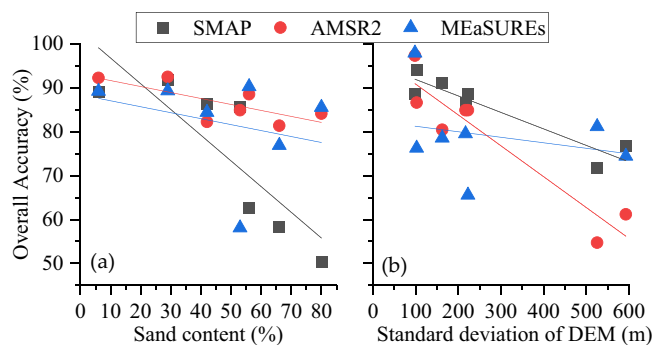

Fig. 14. Relationship between SMAP, AMSR2 and MEaSUREs F/T classification accuracies and sand content (thawing periods over ascending orbits) and elevation standard deviation (thawing periods over descending orbits).

Table 6

False alarm mitigation statistics over the China study domain. A represents the number of false alarm mitigations, and B represents all data numbers.

Orbits	Genhe(A/B)	Saihanba(A/B)	Ngari(A/B)	Naqu(A/B)	Dachaidan(A/B)	Tianjun(A/B)	Qumalai(A/B)	Chengduo(A/B)
Ascending	14/728	2/181	14/364	8/364	47/912	4/912	4/912	7/912
Descending	31/728	1/181	7/364	3/364	20/912	4/912	3/912	3/912

plateau continental and cold climate) (Chan et al., 2018) and terrain (DEM ranges from 150 to 600). Moreover, these four study areas contain records of soil temperature and air temperature, so they can also provide an analysis of similarities and differences of the results validated by soil and air temperature respectively. The scale mismatch of the point-to-area situation in these areas may also account for the poor validation results in these areas.

DFA (Wang et al., 2018) was used for AMSR-E Tb and 5 cm soil temperature of 46 in situ sites including China (CTP-SMTMN), USA (USA_NET, APEX), Canada (FLUXNET) and Finland (FMI) to parameterize the DFA (Zhao et al., 2011). Moreover, the DFA algorithm was validated with the same data set, achieving an overall accuracy of 90.06% (Wang et al., 2018). The findings about the snowmelt influence, in which SMAP was not influenced by snowmelt in the winter while AMSR2 was influenced by it, are findings that are limited to the study area in this paper. The conclusion regarding the climate influence, in which SMAP was most affected by the arid climate, followed by AMSR2, and MEaSUREs, which were almost unaffected by the arid climate, are findings that are restricted to the area in this study. The discovery about the F/T depth of products' representation, indicating that SMAP and AMSR2 F/T products could represent the F/T of 5 cm depth underground soil, but the MEaSUREs F/T product was more likely to describe the surface F/T state, is a conclusion limited to the study undertaken in this paper. For other study areas and other depths of evaluation data, the accuracy of SMAP, AMSR2 and MEaSUREs F/T products may exhibit a different performance. However, this paper provides a reference for the performance of SMAP, AMSR2 and MEaSUREs F/T products in permafrost and seasonal permafrost regions in China.

5. Conclusions

In this study, the performances of SMAP, AMSR2 and MEaSUREs F/T products over different study areas in China were evaluated, including Northeast China, North China and the Tibetan Plateau. The time series consistency among F/T products and in situ soil temperature was analyzed, and the soil temperature was used as validation data to evaluate the accuracies of SMAP, AMSR2 and MEaSUREs F/T products over eight study areas during the freezing and thawing periods. In addition, the air and soil temperatures were used in the evaluation work over four study areas to understand the difference of surface F/T depth represented by three F/T products and the influence of snowmelt. The accuracies of the SMAP and AMSR2 F/T products in nonarid climate areas are higher than that those in arid areas, and there was no obvious difference between freezing and thawing periods. For the SMAP F/T product, when the F/T transition occurs in arid areas, the phase transition water content is too small to reflect the surface seasonal F/T state. For AMSR2 F/T products with dual bands, the inconsistent F/T state indicated by the small phase transition water content and the significant temperature change introduces difficulties to the detection of F/T in arid areas. Since ERA-interim SAT was used as auxiliary data to define the F/T threshold for MEaSUREs, it was less affected by the arid climate type, and the overall accuracy in the arid and nonarid climate type in the study area was not significantly different.

Although there have been some studies for validation of the F/T products of SMAP, AMSR2, and MEaSUREs, most of the studies have been done using soil temperature data from North America and Europe or air temperature data from global weather stations. The validation of

F/T products in China and different climatic zones is not sufficient for the application requirements. We first perform a systematic evaluation and analysis of the performance and influential factors of SMAP (L-band), AMSR2 (Ku- and Ka-band) and MEaSUREs (Ka-band) F/T products in China. Analogous to previous studies, we also found the influence of snowmelt in the spring, but differently, we also found the influence of snowmelt in the winter, with SAMP uninfluenced by snowmelt in the winter, while AMSR2 was influenced by it over QTP. This discovery is very important to improve the F/T detection algorithm in areas without continuous snow cover. We also found the arid climate influence on F/T classification, but unlike previous studies, we found SMAP was most affected by the arid climate due to strong sensitivity to soil moisture, followed by ASMR2, which was caused by the use of the same formula as that used in the global region, and MEaSUREs was almost unaffected by the arid climate because it mostly depended on the air temperature. It is of great significance to the improvement of F/T algorithms and product applications in arid regions. For the first time, we were able to draw the conclusion that SMAP and AMSR2 F/T products could represent the F/T of 5 cm depth underground soil, but the MEaSUREs F/T product was more likely to describe the surface F/T state. According to the analysis of the SMAP F/T algorithm, SMAP NPR is sensitive to soil moisture. Even so, it cannot detect the F/T transition until the change in soil moisture reaches a certain degree (e.g., 0.2 m^3/m^3). F/T products were affected by the soil texture in the particular sand content and spatial heterogeneity of the DEM. Due to the inaccuracy of the reanalysis data and the complexity of the QTP topography, ecology and climate, the F/T detection in the QTP is more unstable for SMAP and MEaSUREs during the summer. The surface F/T state in the midlatitude areas is affected by the shorter annual frozen time and less obvious freezing phenomena than that in boreal forest areas. It is still difficult to obtain an F/T product with better accuracy over that area at present.

In future work, we will improve the F/T algorithm to enhance its sensitivity to both liquid water and temperature changes. Simultaneously, it is necessary to optimize the algorithm for different regions due to the differences in moisture and temperature changes in different regions caused by different climate types, soil texture and other factors.

CRediT authorship contribution statement

Jian Wang: Conceptualization, Methodology, Software, Validation, Writing - original draft.**Lingmei Jiang:**Conceptualization, Supervision, Methodology, Writing - review & editing.**Huizhen Cui:**Methodology, Investigation, Writing - review & editing.**Gongxue Wang:**Methodology, Investigation, Writing - review & editing.**Jianwei Yang:**Methodology, Investigation, Writing - review & editing.**Xiaojing Liu:**Investigation.**Xu Su:**Investigation.

and soil temperature dataset used in Naqu area was provided by Data Assimilation and Modeling Center for Tibetan Multi-spheres, Institute of Tibetan Plateau Research, Chinese Academy of Sciences. We would also like to thank the National Snow and Ice Data Center for providing the SMAP F/T product and JAXA for providing the AMSR2 L3 data.

Declaration of competing interest

The authors declare that they have no known competing financial interests or personal relationships that could have appeared to influence the work reported in this paper.

References

Chai, L.N., Zhang, L.X., Zhang, Y.Y., Hao, Z.G., Jiang, L.M., Zhao, S.J., 2014. Comparison of the classification accuracy of three soil freeze–thaw discrimination algorithms in China using SSMIS and AMSR-E passive microwave imagery. Int. J. Remote Sens. 35, 7631–7649. https://doi.org/10.1080/01431161.2014.975376.

Chan, S.K., Bindlish, R., O'Neill, P., Jackson, T., Kerr, Y., 2018. Development and assessment of the SMAP enhanced passive soil moisture product. Remote Sens. Environ. 204, 931–941. https://doi.org/10.1016/j.rse.2017.08.025.

Chen, J., Chen, J., Liao, A.P., Cao, X., Chen, L.J., Chen, X.H., He, C.Y., Han, G., Peng, S., Lu, M., Zhang, W.W., Tong, X.H., Mills, J., 2015. Global land cover mapping at 30 m resolution: a POK-based operational approach. ISPRS-J. Photogramm. Remote Sens. 103, 7–27. https://doi.org/10.1016/j.isprsjprs.2014.09.002.

Chen, T., Zhi, H., Bian, D., 2019. Investigation on the discrepancy between observed surface temperature and ERA-interim over the Qinghai-Tibet Plateau and its attribution. J. Mt. Sci. 37, 1–8. https://doi.org/10.16089/j.cnki.1008-2786.000393.

Christensen, T.R., 2016. It's a gas. Nat. Geosci. 9, 647–648. https://doi.org/10.1038/ngeo2803.

Colliander, A., Mcdonald, K., Zimmermann, R., Schroeder, R., Kimball, J.S., Njoku, E.G., 2012. Application of QuikSCAT backscatter to SMAP validation planning: freeze/thaw state over ALECTRA sites in Alaska from 2000 to 2007. IEEE Transactions on Geoscience Remote Sensing 50, 461–468. https://doi.org/10.1109/TGRS.2011.2174368.

Cui, Y., Wang, C.H., 2009. Comparison of sensible and latent heat fluxes during the transition season over the western Tibetan Plateau from reanalysis datasets. Prog. Nat. Sci. 19, 719–726. https://doi.org/10.1016/j.pnsc.2008.11.001.

Cui, H.Z., Jiang, L.M., Du, J.Y., Zhao, S.J., Wang, G.X., Lu, Z., Wang, J., 2017. Evaluation and analysis of AMSR-2, SMOS, and SMAP soil moisture products in the Genhe area of China. Journal of Geophysical Research Atmospheres 122, 8650–8666. https://doi.org/10.1002/2017jd026800.

Davitt, A., Schumann, G., Forgotson, C., McDonald, K.C., 2019. The utility of SMAP soil moisture and freeze-thaw datasets as precursors to spring-melt flood conditions: a case study in the Red River of the North Basin. IEEE Journal of Selected Topics in Applied Earth Observations and Remote Sensing 1–14. https://doi.org/10.1109/JSTARS.2019.2918947.

Derksen, C., Xu, X.L., Dunbar, R.S., Colliander, A., Kim, Y., Kimball, J.S., Black, T.A., Euskirchen, E., Langlois, A., Loranty, M.M., 2017. Retrieving landscape freeze/thaw state from Soil Moisture Active Passive (SMAP) radar and radiometer measurements. Remote Sens. Environ. 194, 48–62. https://doi.org/10.1016/j.rse.2017.03.007.

Du, J.Y., Kimball, J.S., Azarderakhsh, M., Dunbar, R.S., Moghaddam, M., McDonald, K.C., 2015. Classification of Alaska spring thaw characteristics using satellite L-band radar remote sensing. IEEE Transactions on Geoscience Remote Sensing 53, 542–556. https://doi.org/10.1109/TGRS.2014.2325409.

Edwards, A.C., Scalenghe, R., Freppaz, M., 2007. Changes in the seasonal snow cover of alpine regions and its effect on soil processes: a review. Quat. Int. 162, 172–181. https://doi.org/10.1016/j.quaint.2006.10.027.

Gabrielle, W., 2007. Climate change 2007: a world melting from the top down. Nature 446, 718–721. https://doi.org/10.1038/446718a.

Han, M.L., Yang, K., Qin, J., Jin, R., Ma, Y.M., Wen, J., Chen, Y.Y., Zhao, L., Lazhu, Tang, W.J.,2015. An algorithm based on the standard deviation of passive microwave brightness temperatures for monitoring soil surface freeze/thaw state on the Tibetan Plateau. IEEE Transactions on Geoscience Remote Sensing. 53, 2775–2783. doi:https://doi.org/10.1109/TGRS.2014.2364823.

Hu, T.X., Zhao, T.J., Zhao, K.G., Shi, J.C., 2019. A continuous global record of near-surface soil freeze/thaw status from AMSR-E and AMSR2 data. Int. J. Remote Sens. 40, 6993–7016. https://doi.org/10.1080/01431161.2019.1597307.

Jiang, L.M., Xu, W.X., Zhang, J., Wang, G.X., Liu, X.J., Zhao, S.J., 2017. An automatic measurement dataset on the snow depth in the Tibetan Plateau (2015–2016). Science China Data 2, 1–9. https://doi.org/10.11922/csdata.170.2017.0116.

Jin, R., Li, X., Che, T., 2009. A decision tree algorithm for surface soil freeze/thaw classification over China using SSM/I brightness temperature. Remote Sens. Environ. 113, 2651–2660. https://doi.org/10.1016/j.rse.2009.08.003.

Jin, R., Zhang, T.J., Li, X., Yang, X.G., Ran, Y.H., 2015. Mapping surface soil freeze-thaw cycles in China based on SMMR and SSM/I brightness temperatures from 1978 to 2008. Arct. Antarct. Alp. Res. 47, 213–229. https://doi.org/10.1657/AAAR00C-13-304.

Judge, J., Galantowicz, J.F., England, A.W., Dahl, P., 1997. Freeze/thaw classification for prairie soils using SSM/I radiobrightnesses. In: IEEE International Symposium on Geoscience and Remote Sensing.Singapore, pp. 827–832. https://doi.org/10.1109/36.602525.

Kim, Y., Kimball, J.S., Mcdonald, K.C., Glassy, J., 2011a. Developing a global data record of daily landscape freeze/thaw status using satellite passive microwave remote sensing. IEEE Transactions on Geoscience Remote Sensing 49, 949–960. https://doi.org/10.1109/TGRS.2010.2070515.

Kim, Y., Kimball, J.S., Zhang, K., Mcdonald, K.C., 2011b. Satellite detection of northern hemisphere non-frozen season changes and associated impacts to vegetation growing seasons. In: Agu Fall Meeting.San Francisco, pp. 602. http://adsabs.harvard.edu/abs/2011AGUFM.B51M0602K.

Kim, Y., Kimball, J.S., Zhang, K., Mcdonald, K.C., 2012. Satellite detection of increasing Northern Hemisphere non-frozen seasons from 1979 to 2008: implications for regional vegetation growth. Remote Sens. Environ. 121, 472–487. https://doi.org/10.1016/j.rse.2012.02.014.

Kim, Y., Kimball, J.S., Glassy, J., Du, J.Y., 2017. An extended global earth system data record on daily landscape freeze-thaw status determined from satellite passive microwave remote sensing. Earth System Science Data 9, 133–147. https://doi.org/10.5194/essd-9-133-2017.

Kim, Y., Kimball, J.S., Xu, X., Dunbar, R.S., Colliander, A., Derksen, C., 2019. Global assessment of the SMAP freeze/thaw data record and regional applications for detecting spring onset and frost events. Remote Sens. 11, 1317. https://doi.org/10.3390/rs11111317.

Kimball, J.S., Mcdonald, K.C., Keyser, A.R., Frolking, S., Running, S.W., 2001. Application of the NASA Scatterometer (NSCAT) for determining the daily frozen and nonfrozen landscape of Alaska. Remote Sens. Environ. 75, 113–126. https://doi.org/10.1016/S0034-4257(00)00160-7.

Kimball, J.S., Mcdonald, K.C., Frolking, S.E., Running, S.W., 2004a. Radar remote sensing of the spring thaw transition across a boreal landscape. Remote Sens. Environ. 89, 163–175. https://doi.org/10.1016/j.rse.2002.06.004.

Kimball, J.S., Mcdonald, K.C., Running, S.W., Frolking, S.E., 2004b. Satellite radar remote sensing of seasonal growing seasons for boreal and subalpine evergreen forests. Remote Sens. Environ. 90, 243–258. https://doi.org/10.1016/j.rse.2004.01.002.

Kou, X.K., Jiang, L.M., Yan, S., Zhao, T.J., Lu, H., Cui, H.Z., 2017. Detection of land surface freeze-thaw status on the Tibetan Plateau using passive microwave and thermal infrared remote sensing data. Remote Sens. Environ. 199, 291–301. https://doi.org/10.1016/j.rse.2017.06.035.

Kou, X.K., Jiang, L.M., Yan, S., Wang, J., Gao, L.Y., 2018. Research on the improvement of passive microwave freezing and thawing discriminant algorithms for complicated surface conditions. In: IEEE International Symposium on Geoscience and Remote Sensing.Valencia, pp. 7161–7164. https://doi.org/10.1109/IGARSS.2018.8518731.

Li, L., Li, H.M., Shen, H.Y., Liu, C.H., Ma, Y.C., Zhao, Y.C., 2018. The truth and inter-annual oscillation causes for climate change in the Qinghai-Tibet Plateau. J. Glaciol. Geocryol. 40, 1079–1089. https://doi.org/10.7522/j.issn.1000-0240.2018.0117.

Li, X.D., Shao, M.A., Zhao, C.L., Liu, T., Jia, X.X., Ma, C.K., 2019. Regional spatial variability of root-zone soil moisture in arid regions and the driving factors - a case study of Xinjiang, China. Can. J. Soil Sci. 99, 277–291. https://doi.org/10.1139/cjss-2019-0006.

Liu, X.D., Chen, B.D., 2000. Climatic warming in the Tibetan plateau during recent decades. Int. J. Climatol. 20, 1729–1742. https://doi.org/10.1002/1097-0088(20001130)20:14<1729::AID-JOC556>3.0.CO;2-Y.

Liu, J.F., Chen, R.S., 2011. Studying the spatiotemporal variation of snow-covered days over China based on combined use of MODIS snow-covered days and in situ observations. Theor. Appl. Climatol. 106, 355–363. https://doi.org/10.1007/s00704-011-0441-9.

Lyu, H.B., McColl, K.A., Li, X.L., Derksen, C., Berg, A., Black, T.A., Euskirchen, E., Loranty, M., Pulliainen, J., Rautiainen, K., Rowlandson, T., Roy, A., Royer, A., Langlois, A., Stephens, J., Lu, H., Entekhabi, D., 2018. Validation of the SMAP freeze/thaw product using categorical triple collocation. Remote Sens. Environ. 205, 329–337. https://doi.org/10.1016/j.rse.2017.12.007.

Mao, J.F., Shi, X.Y., Ma, L.J., Kaiser, D.P., Li, Q.X., Thornton, P.E., 2010. Assessment of reanalysis daily extreme temperatures with China's homogenized historical dataset during 1979–2001 using probability density functions. J. Clim. 23, 6605–6623. https://doi.org/10.1175/2010jcli3581.1.

McDonald, K.C., Kimball, J.S., 2005. Estimation of surface freeze–thaw states using microwave sensors. In: Anderson, M.G. (Ed.), Encyclopedia of Hydrological Sciences. Wiley, J., Sons Ltd, West Sussex, pp. 783–797. https://doi.org/10.1002/0470848944.hsa059a.

Mcdonald, K.C., Kimball, J.S., Njoku, E., Zimmermann, R., Zhao, M., 2004. Variability in springtime thaw in the terrestrial high latitudes: monitoring a major control on the biospheric assimilation of atmospheric CO_2 with spaceborne microwave remote sensing. Earth Interact. 8, 1. https://doi.org/10.1175/1087-3562(2004)82.0.CO;2.

Mcfarland, M.J., Miller, R.L., Neale, C.M.U., 1990. Land surface temperature derived from the SSM/I passive microwave brightness temperatures. IEEE Transactions on Geoscience Remote Sensing 28, 839–845. https://doi.org/10.1109/36.58971.

MIing, S.H., Qin, Z.K., Huang, Y., 2019. Climate trend of upper troposphere temperature revealed by satellite data over the Qinghai-Tibetan Plateau. Plateau Meteorology 38, 264–277. https://doi.org/10.7522/j.issn.1000-0534.2018.00120.

Mironov, V.L., Kerr, Y.H., Kosolapova, L.G., Savin, I.V., Muzalevskiy, K.V., 2015. A temperature-dependent dielectric model for thawed and frozen organic soil at 1.4 GHz. IEEE Journal of Selected Topics in Applied Earth Observations and Remote Sensing 8, 4470–4477. https://doi.org/10.1109/JSTARS.2015.2442295.

Parinussa, R.M., Holmes, T.R.H., Yilmaz, M.T., Crow, W.T., 2011. The impact of land surface temperature on soil moisture anomaly detection from passive microwave observations. Hydrol. Earth Syst. Sci. 15, 3135–3151. https://doi.org/10.5194/hess-15-3135-2011.

Qin, J., Yang, K., Liang, S.L., Guo, X.F., 2009. The altitudinal dependence of recent rapid warming over the Tibetan Plateau. Clim. Chang. 97, 321–327. https://doi.org/10.

1007/s10584-009-9733-9.

Qin, J., Yang, K., Lu, N., Chen, Y.Y., Zhao, L., Han, M.L., 2013. Spatial upscaling of in-situ soil moisture measurements based on MODIS-derived apparent thermal inertia. Remote Sens. Environ. 138, 1–9. https://doi.org/10.1016/j.rse.2013.07.003.

Qiu, G.Q., Zhou, Y.W., Guo, D.X., Wang, Y.X., 2000. Map of Geocryological Regions and Classifications. http://westdc.westgis.ac.cn/data/15bf484c-e4bc-4990-b01b-c26da686e254.

Rautiainen, K., Lemmetyinen, J., Schwank, M., Kontu, A., Ménard, C.B., Mätzler, C., Drusch, M., Wiesmann, A., Ikonen, J., Pulliainen, J., 2014. Detection of soil freezing from L-band passive microwave observations. Remote Sens. Environ. 147, 206–218. https://doi.org/10.1016/j.rse.2014.03.007.

Rautiainen, K., Parkkinen, T., Lemmetyinen, J., Schwank, M., Wiesmann, A., Ikonen, J., Derksen, C., Davydov, S., Davydova, A., Boike, J., 2016. SMOS prototype algorithm for detecting autumn soil freezing. Remote Sens. Environ. 180, 346–360. https://doi.org/10.1016/j.rse.2016.01.012.

Rautiainen, K., Lemmetyinen, J., Aalto, T., Tsuruta, A., Kangasaho, V., Ikonen, J., Cohen, J., Kontu, A., Vehvildäinen, J., Pulliainen, J., 2018. Smos retrievals of soil freezing and thawing and its applications. In: IEEE International Geoscience and Remote Sensing Symposium.Valencia, pp. 1463–1465. https://doi.org/10.1109/IGARSS.2018.8519243.

Roy, A., Royer, A., Derksen, C., Brucker, L., Langlois, A., Mialon, A., Kerr, Y.H., 2015. Evaluation of spaceborne L-band radiometer measurements for terrestrial freeze/thaw retrievals in Canada. IEEE Journal of Selected Topics in Applied Earth Observations and Remote Sensing 8, 4442–4459. https://doi.org/10.1109/JSTARS.2015.2476358.

Roy, A., Toose, P., Derksen, C., Rowlandson, T., Sonnentag, O., 2017a. Spatial variability of L-band brightness temperature during freeze/thaw events over a prairie environment. Remote Sens. 9, 894. https://doi.org/10.3390/rs9090894.

Roy, A., Toose, P., Williamson, M., Rowlandson, T., Derksen, C., Royer, A., Berg, A.A., Lemmetyinen, J., Arnold, L., 2017b. Response of L-band brightness temperatures to freeze/thaw and snow dynamics in a prairie environment from ground-based radiometer measurements. Remote Sens. Environ. 191, 67–80. https://doi.org/10.1016/j.rse.2017.01.017.

Running, S.W., Mcdonald, K.C., Kimball, J.S., Frolking, S., Keyser, A.R., Zimmerman, R., 1999. Radar remote sensing proposed for monitoring freeze-thaw transitions in boreal regions. Transactions, American Geophysical Union 80, 213–221. https://doi.org/10.1029/99EO00158.

Schuur, E.A.G., Abbott, B., 2011. High risk of permafrost thaw. Nature 480, 32–33. https://doi.org/10.1038/480032a.

Su, Z., Wen, J., Dente, L., Velde, R.V.D., Wang, L., Ma, Y., Yang, K., Hu, Z., 2011. The Tibetan Plateau observatory of plateau scale soil moisture and soil temperature (Tibet-Obs) for quantifying uncertainties in coarse resolution satellite and model products. Hydrol. Earth Syst. Sci. 15, 2303–2316. https://doi.org/10.5194/hess-15-2303-2011.

Swindles, G.T., Morris, P.J., Mullan, D., Watson, E.J., Turner, T.E., Roland, T.P., Amesbury, M.J., Kokfelt, U., Schoning, K., Pratte, S., Gallego-Sala, A., Charman, D.J., Sanderson, N., Garneau, M., Carrivick, J.L., Woulds, C., Holden, J., Parry, L., Galloway, J.M., 2015. The long-term fate of permafrost peatlands under rapid climate warming. Sci. Rep. 5, 17951. https://doi.org/10.1038/srep17951.

Wang, H.Y., Liang, C., 2013. Climatic change in Qinghai-Tibet Plateau and the surrounding areas in 130 years. Meteorological and Environmental Research 35, 4–9. https://doi.org/10.1080/07036337.2013.774778.

Wang, J.Y., Song, C.C., Hou, A.X., Xi, F.M., 2017a. Methane emission potential from freshwater marsh soils of Northeast China: response to simulated freezing-thawing cycles. Wetlands 37, 437–445. https://doi.org/10.1007/s13157-017-0879-3.

Wang, T.J., Franz, T.E., Li, R.P., You, J.S., Shulski, M.D., Ray, C., 2017b. Evaluating climate and soil effects on regional soil moisture spatial variability using EOFs. Water Resour. Res. 53, 4022–4035. https://doi.org/10.1002/2017wr020642.

Wang, T.J., Liu, Q., Franz, T.E., Li, R.P., Lang, Y.C., Fiebrich, C.A., 2017c. Spatial patterns of soil moisture from two regional monitoring networks in the United States. J. Hydrol. 552, 578–585. https://doi.org/10.1016/j.jhydrol.2017.07.035.

Wang, P.K., Zhao, T.J., Shi, J.C., Hu, T.X., Roy, A., Qiu, Y.B., Lu, H., 2018. Parameterization of the freeze/thaw discriminant function algorithm using dense in-situ observation network data. International Journal of Digital Earth 12, 980–994. https://doi.org/10.1080/17538947.2018.1452300.

Williamson, M., Rowlandson, T.L., Berg, A.A., Roy, A., Toose, P., Derksen, C., Arnold, L., Tetlock, E., 2018. L-band radiometry freeze/thaw validation using air temperature and ground measurements. Remote Sensing Letters 9, 403–410. https://doi.org/10.1080/2150704X.2017.1422872.

Xu, X.L., Dunbar, R.S., Derksen, C., Colliander, A., Kim, Y., Kimball, J.S., 2018. SMAP L3 Radiometer Global and Northern Hemisphere Daily 36 km EASE-Grid Freeze/Thaw State. 2https://doi.org/10.5067/YN94K53QM061.

Yang, K., Qin, J., Zhao, L., Chen, Y.Y., Tang, W.J., Han, M.L., Lazhu, Chen, Z.Q., Lv, N., Ding, B.H., 2013. A multi-scale soil moisture and freeze-thaw monitoring network on the third pole. Bull. Amer. Meteorol. Soc. 94, 1907–1916. https://doi.org/10.1175/BAMS-D-12-00203.1.

Yang, H.J., Li, Y.N., Zhang, Z.D., Xu, Z.Q., Huang, X.R., 2019. GIS-based multi-criteria assessment and seasonal impact on plantation forest landscape visual sensitivity. Forests 10, 297. https://doi.org/10.3390/f10040297.

Zhang, T.J., Armstrong, R.L., 2001. Soil freeze/thaw cycles over snow-free land detected by passive microwave remote sensing. Geophys. Res. Lett. 28, 763–766. https://doi.org/10.1029/2000GL011952.

Zhang, T.J., Zhong, X.Y., 2014. Classification and regionalization of the seasonal snow cover across the Eurasian continent. J. Glaciol. Geocryol. 36, 481–490. https://doi.org/10.7522/j.issn.1000-0240.2014.0058.

Zhang, L.X., Shi, J.C., Zhang, Z.J., Zhao, K.G., 2003a. The estimation of dielectric constant of frozen soil-water mixture at microwave bands. In: IEEE International Symposium on Geoscience and Remote Sensing.FRANCE, pp. 2903–2905. https://doi.org/10.1109/IGARSS.2003.1294626.

Zhang, T.J., Armstrong, R.L., Smith, J., 2003b. Investigation of the near-surface soil freeze-thaw cycle in the contiguous United States: algorithm development and validation. Journal of Geophysical Research Atmospheres 108, 8860. https://doi.org/10.1029/2003JD003530.

Zhao, T.J., Zhang, L.X., Jiang, L.M., Zhao, S.J., Chai, L.N., Jin, R., 2011. A new soil freeze/thaw discriminant algorithm using AMSR-E passive microwave imagery. Hydrol. Process. 25, 1704–1716. https://doi.org/10.1002/hyp.7930.

Zhao, T., Shi, J., Hu, T., Zhao, L., Zou, D., Wang, T., Ji, D., Li, R., Wang, P., 2017. Estimation of high-resolution near-surface freeze/thaw state by the integration of microwave and thermal infrared remote sensing data on the Tibetan Plateau. Earth and Space Science 4 (8), 4 (2017-08-05).

Zhou, Y.W., Guo, D.X., 1982. Principal characteristics of permafrost in China. J. Glaciol. Geocryol. 4, 1–19. http://www.bcdt.ac.cn/CN/Y1982/V4/I1/1.

Zuerndorfer, B., England, A.W., 1992. Radiobrightness decision criteria for freeze/thaw boundaries. IEEE Transactions on Geoscience Remote Sensing 30, 89–102. https://doi.org/10.1109/36.124219.

Zuerndorfer, B.W., England, A.W., Dobson, M.C., Ulaby, F.T., 1990. Mapping freeze/thaw boundaries with SMMR data. Agric. For. Meteorol. 52, 199–225. https://doi.org/10.1016/0168-1923(90)90106-G.